APL Materials

RESEARCH ARTICLE | NOVEMBER 02 2026

High-mobility La-doped $BaSnO_3$ thin films with sheet carrier concentrations relevant to transistors

Nicholas A. Parker ; Seungmin Lee ; Adedapo Oni; George N. Kotsonis ; Kathy Azizie ; Jisung Park ; Hanjong Paik ; Jacary Sapp ; Jay R. Wright; D. Jena ; H. G. Xing ; Dmitri A. Tenne ; Punyashloka Debashis ; Pratyush Buragohain ; Raseong Kim ; Rachel Steinhardt; Darrell G. Schlom

Check for updates

APL Mater. 14, 111101 (2026)
https://doi.org/10.1063/5.0296731

View Online
Export Citation

Articles You May Be Interested In

Scattering mechanisms and mobility enhancement in epitaxial $BaSnO_3$ thin films probed via electrolyte gating

APL Mater. (July 2020)

Gd-doped $BaSnO_3$: A transparent conducting oxide with localized magnetic moments

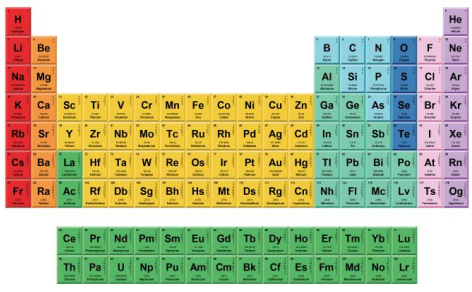
Appl. Phys. Lett. (January 2016)

Enhanced electron mobility at the two-dimensional metallic surface of $BaSnO_3$ electric-double-layer transistor at low temperatures

Appl. Phys. Lett. (May 2017)

08 November 2026 01:46:08

AMERICAN ELEMENTS
THE MATERIALS SCIENCE MANUFACTURER®
Now Invent.™
29th ANNIVERSARY 1997 – 2026



American Elements
Opens a World of Possibilities
...Now Invent!
www.americanelements.com
© 1997-2026. American Elements is a U.S. Registered Trademark

AIP Publishing

High-mobility La-doped $BaSnO_3$ thin films with sheet carrier concentrations relevant to transistors

Cite as: APL Mater. 14, 111101 (2026); doi: 10.1063/5.0296731
Submitted: 14 August 2025 • Accepted: 13 October 2026 •
Published Online: 2 November 2026

View Online Export Citation CrossMark

Nicholas A. Parker,[1] Seungmin Lee,[1] Adedapo Oni,[2] George N. Kotsonis,[1] Kathy Azizie,[1] Jisung Park,[1] Hanjong Paik,[1,3,4] Jacary Sapp,[1] Jay R. Wright,[5] D. Jena,[1,6,7] H. G. Xing,[1,6,7] Dmitri A. Tenne,[5] Punyashloka Debashis,[8] Pratyush Buragohain,[8] Raseong Kim,[8] Rachel Steinhardt,[8] and Darrell G. Schlom[1,7,9,a)]

AFFILIATIONS

[1] Department of Materials Science and Engineering, Cornell University, Ithaca, New York 14853, USA
[2] Intel Foundry Quality and Reliability, Hillsboro, Oregon 97124, USA
[3] School of Electrical and Computer Engineering, University of Oklahoma, Norman, Oklahoma 73019, USA
[4] Center for Quantum Research and Technology, University of Oklahoma, Norman, Oklahoma 73019, USA
[5] Department of Physics and Astronomy, Boise State University, Boise, Idaho 83725, USA
[6] School of Electrical and Computer Engineering, Cornell University, Ithaca, New York 14853, USA
[7] Kavli Institute at Cornell for Nanoscale Science, Ithaca, New York 14853, USA
[8] Intel Foundry Technology Research, Hillsboro, Oregon 97124, USA
[9] Leibniz-Institut für Kristallzüchtung, Max-Born-Str. 2, Berlin 12489, Germany

[a)] **Author to whom correspondence should be addressed:** schlom@cornell.edu

08 November 2026 01:46:08

ABSTRACT

With demonstrated room-temperature mobilities in single crystals and thin films exceeding 300 $cm^2\ V^{-1}\ s^{-1}$ and 180 $cm^2\ V^{-1}\ s^{-1}$, respectively, the transparent conducting oxide La-doped $BaSnO_3$ is of great interest for electronics. Unfortunately, the sheet carrier concentration of the films in which such high mobilities are achieved exceeds 6×10^{13} cm^{-2}, which is too high to be pinched off in most transistor structures. Here, we investigate more than 200 La-doped $BaSnO_3$ films grown on (100) MgO with lower sheet carrier concentrations—in the (1–6) $\times 10^{13}$ cm^{-2} range—to elucidate the mobilities that can be achieved in the channel layers of transistors that have a chance of being pinched off. Our study provides information on how the mobility trades off with film thickness and doping within this device-relevant design space. The La-doped $BaSnO_3$ films were grown by suboxide molecular-beam epitaxy in an adsorption-controlled regime, with excess SnO provided during growth and exhibit carrier concentrations on the order of 1×10^{19} cm^{-3}, thicknesses ranging from 5 to 38 nm, surfaces with rms roughness <1 nm, and mobilities as high as 106 $cm^2\ V^{-1}\ s^{-1}$ at room temperature. The fraction of lanthanum dopants that are electrically active ranges from 40% to 68%; this fraction increases with increasing SnO excess (the SnO:Ba flux ratio) during growth.

© 2026 Author(s). All article content, except where otherwise noted, is licensed under a Creative Commons Attribution-NonCommercial-NoDerivs 4.0 International (CC BY-NC-ND) license (https://creativecommons.org/licenses/by-nc-nd/4.0/). https://doi.org/10.1063/5.0296731

INTRODUCTION

La-doped $BaSnO_3$ has long been identified as a premier transparent conducting oxide (TCO) for implementation into oxide-based transistor devices.[1,2] This can be attributed to the demonstrated high mobility (μ) at room temperature,[1–11] n-type conductivity up to ~800 °C in dry air,[1,12] and visible light transparency due to a wide bandgap of ~3.0 eV.[2,5,13,14] In particular, single crystals have demonstrated mobilities as high as 320 $cm^2\ V^{-1}\ s^{-1}$ in a degenerately doped regime ($n = 8 \times 10^{19}\ cm^{-3}$),[1] and at comparable carrier densities, thin films have shown mobilities in excess of 180 $cm^2\ V^{-1}\ s^{-1}$.[6,10] These high mobilities out compete current industrial semiconductor materials of choice, including Si, Ge, GaAs, and GaN, at carrier concentrations exceeding $5 \times 10^{19}\ cm^{-3}$.[15,16] Other TCOs exist with lower mobilities at this carrier concentration level and comparable bandgaps, such as ZnO[17] and indium-tin oxide.[18] The only known TCO with a higher electron mobility in this doping range is CdO[19] albeit with toxicity issues that, coupled with its lower bandgap of ~2.3 eV,[20,21] make it less attractive than $BaSnO_3$.

The challenge with utilizing La-doped $BaSnO_3$ as a channel material in a transistor structure, however, is that the record mobilities exceeding 180 $cm^2\ V^{-1}\ s^{-1}$ have only been achieved in films with high sheet carrier concentrations (n_s). For example, Paik *et al.*[6] achieved a mobility of 183 $cm^2\ V^{-1}\ s^{-1}$ in a film with a sheet carrier density of $7 \times 10^{14}\ cm^{-2}$, and Park *et al.*[10] achieved a mobility of 184 $cm^2\ V^{-1}\ s^{-1}$ in a film with a sheet carrier density of $6 \times 10^{13}\ cm^{-2}$. Furthermore, these highly doped layers were grown on thick (150–330 nm) unintentionally doped (UID) $BaSnO_3$ buffer layers, which are likely not compatible with modern non-planar transistor structures. Nevertheless, the presence of these semiconductor properties coinciding with a widely applicable perovskite structure makes La-doped $BaSnO_3$ a choice candidate for use in epitaxially grown oxide perovskite transistors. In fact, many transistor structures, including La-doped $BaSnO_3$ channel layers, have been reported,[10,22–31] although with field-effect mobilities far lower than those mentioned above.

Several strategies have been used in the fabrication of La-doped $BaSnO_3$-based transistors to date. One is to use gate dielectrics with a high product of κ (dielectric constant) × E_{BD} (electrical breakdown field), e.g., HfO_2,[10,23,25] $LaInO_3$,[24] $SrHfO_3$,[30] $BaHfO_3$,[26] $BaTiO_3$,[32] or $BaHf_{0.6}Ti_{0.4}O_3$[29] to deplete the conducting channel of La-doped $BaSnO_3$. This approach has enabled channels with sheet carrier densities as high as $1 \times 10^{14}\ cm^{-2}$ to be pinched off.[29] Another approach is to use the spontaneous polarization (P_s) of a ferroelectric such as $Pb(Zr,Ti)O_3$ to deplete the channel.[31,33] So far, the $Pb(Zr,Ti)O_3$ approach has achieved a charge modulation on a La-doped $BaSnO_3$ channel of only $7 \times 10^{12}\ cm^{-2}$.[31] In principle, were it not for interface traps and depolarization fields, $Pb(Zr,Ti)O_3$ with $P_s = 50\ \mu C\ cm^{-2}$ should be able to deplete a sheet carrier density of $3 \times 10^{14}\ cm^{-2}$. A third approach is to decrease the sheet carrier density of the channel. This approach would seem to be the most straightforward, but here the challenge is that the electron mobility plummets as the sheet carrier density is decreased,[3,10,23,34] which often leads to insulating films despite the presence of lanthanum dopants at concentrations exceeding $1 \times 10^{19}\ cm^{-3}$.[9,23,34,35]

This third approach, where we reduce the sheet carrier density of the La-doped $BaSnO_3$ layer to produce a channel layer suitable for depletion in a high-performance transistor at device-relevant scale, is the focus of this paper. To make progress on this third approach, we consider what it is that has limited scaling the sheet carrier density, by reducing the thickness of the La-doped $BaSnO_3$ layer, its doping, or both, in prior studies in order to identify a way forward. We attribute the loss of conductivity to the point where the concentration of traps in the La-doped $BaSnO_3$ film exceeds the concentration of dopants; all potentially mobile carriers are trapped. Possible traps, such as threading dislocations, have been explored previously in La-doped $BaSnO_3$ films[1,7,34] as well as other semiconductors containing high dislocation densities (Ge,[36,37] Si,[38] GaN,[39] and InSb[40])—with the mobility of all these systems following $\mu \propto \sqrt{n}$.[1,6,34,37–40]

Conceptually, minimizing the threading dislocation density (TDD) in the conducting channel of La-doped $BaSnO_3$ should lead to fewer scattering sites for mobile carriers. Indeed, transparent field-effect transistors based on La-doped $BaSnO_3$ employ thick UID $BaSnO_3$ buffer layers in the heterostructure to maximize the mobility of carriers in the conducting channel, leading to benchmark performance.[10] Microscopy studies of similarly grown La-doped $BaSnO_3$ layers reveal the presence of 10^{10}–$10^{11}\ cm^{-2}$ threading dislocations despite the thick UID $BaSnO_3$ buffer layers employed.[6,8,10,25] More recent studies have investigated the use of buffer layers that are closely lattice-matched to $BaSnO_3$, grown at high temperature to produce relaxed buffer layers with reduced TDD of ~$10^9\ cm^{-2}$. Unfortunately, the resulting thin films of La-doped $BaSnO_3$ grown still do not reach their single crystal mobilities.[8,41] Beyond this, other defects have been suggested that may also impact the mobile carrier concentration of La-doped $BaSnO_3$, such as point defects[6,42–44] and $(BaO)_2$ crystallographic shear defects.[6,45]

To this end, we map out growth conditions for the deposition technique that has, to date, produced La-doped $BaSnO_3$ with the highest mobility in thin films: suboxide molecular-beam epitaxy (*S*-MBE) under adsorption-controlled growth conditions. In thick La-doped $BaSnO_3$ films, this technique has achieved mobilities as high as 184 $cm^2\ V^{-1}\ s^{-1}$ on (100) MgO substrates with thick UID $BaSnO_3$ buffer layers.[10] Using this same substrate, (100) MgO, we explore the influence of La-doped $BaSnO_3$ film thickness and doping density to show the trade-off between electron mobility and sheet carrier density. We observe the highest mobilities at the lowest sheet carrier concentrations ever reported for La-doped $BaSnO_3$ films. The improvement in reported properties is especially clear for the case of no or thin (≤20 nm thick) unintentionally doped $BaSnO_3$ layers under the La-doped $BaSnO_3$ channel. For example, the highest Hall mobility reported to date for a La-doped $BaSnO_3$ film with no underlying UID layer with $n_s < 8 \times 10^{14}\ cm^{-2}$ is ~70 $cm^2\ V^{-1}\ s^{-1}$.[46] We achieve a mobility of 106 $cm^2\ V^{-1}\ s^{-1}$ at more than an order of magnitude lower n_s ($n_s = 6.01 \times 10^{13}\ cm^{-2}$) with no UID layer.

EXPERIMENTAL

La-doped $BaSnO_3$ films were synthesized in a Veeco GEN 10 MBE system using inorganic precursors of lanthanum (99.996% purity, Ames Lab) loaded into a 10 cc tungsten crucible, barium

08 November 2026 01:46:08

© Author(s) 2026

(99.99% purity, Sigma-Aldrich) contained within a 40 cc titanium crucible, and SnO_2 (99.996% purity, Alfa Aesar) in a 40 cc alumina crucible. Film growth occurred by codeposition of lanthanum, barium, SnO (the dominant species emanating from the heated SnO_2 source[6]), and ozone, as described elsewhere.[6] Three ratios of SnO to barium were used, 1.2:1, 2:1, and 4:1. The SnO:Ba ratio was measured by a quartz crystal microbalance (QCM). For each of the three SnO:Ba flux ratios used, the substrate temperature and oxidant pressure were modified to remain within the adsorption-controlled growth window of La-doped $BaSnO_3$. In this window, the sticking coefficient of lanthanum and barium are nominally unity and excess SnO desorbs to form single-phase La-doped $BaSnO_3$.

The substrate temperature was controlled by closed-loop feedback from a thermocouple to the substrate heater power supply and monitored by an optical pyrometer operating at a wavelength of 980 nm. The substrate temperature was kept within 5 °C of the target growth temperature measured by the optical pyrometer by actively lowering the thermocouple setpoint during the growth. The partial pressure of the ~10% ozone plus 90% oxygen mixture, produced by a commercial ozone generator,[47] was set by a heated Baratron capacitance manometer (stabilized at 40 °C) measuring the pressure at the inlet of the ozone nozzle. A fixed MBE chamber background partial pressure of ozone was established for all three SnO:Ba ratios at 5×10^{-7} Torr (i.e., with the SnO source cold the total background pressure of the ~10% ozone plus 90% oxygen mixture was 5×10^{-7} Torr). As the temperature of the SnO source is increased the SnO flux increases, as well as the partial pressure of O_2 emanating from the suboxide source,[6] altering the background pressure of the MBE chamber. Higher fluxes (1.2×10^{14} molecules cm^{-2} s^{-1} for the 4:1 ratio) of SnO coincide with chamber pressures of ~1.2×10^{-6} Torr or lower with an ozone mixture supplied with the same Baratron pressure at the inlet of the ozone nozzle, while lower fluxes (~3.6×10^{13} molecules cm^{-2} s^{-1} for the 1.2:1) maintained the noted 7×10^{-7} Torr chamber pressure from Paik *et al.*[6] The intermediate 2:1 ratio of SnO:Ba used a SnO flux of 6.2×10^{14} molecules cm^{-2} s^{-1} and a background chamber pressure of 9×10^{-7} Torr.

All films were grown on (100) MgO substrates, as provided by the manufacturer, CrysTec GmbH. To facilitate substrate heating by a SiC filament, 20 nm of titanium was evaporated onto the backside of the substrate, followed by 200 nm of platinum. Growths including a UID $BaSnO_3$ buffer layer on the MgO substrate were made by co-supplying fluxes of barium and SnO. Following this, the lanthanum shutter was opened, leading to all sources being co-supplied for the remainder of the growth. Samples that contain no UID $BaSnO_3$ layer had the lanthanum shutter open simultaneously with the barium and SnO_2 shutters at the beginning of growth. In both cases, no post-anneal procedure was done on the samples.

Determining the optimal growth condition for single-phase La-doped $BaSnO_3$ on (100) MgO substrates starts with *in situ* reflection high-energy electron diffraction (RHEED) where observations of secondary phase precipitates and diffuse RHEED patterns allow for minor adjustments in real time to the targeted flux ratio of SnO to barium.[6] *Ex-situ* x-ray diffraction (XRD) was done using Cu $K\alpha_1$ radiation produced from a copper anode in a PANalytical Empyrean system with a hybrid incident-beam monochromator. This XRD was utilized to assess the structural perfection and phase purity of the samples. X-ray reflectivity (XRR) measurements using the same system were used to determine the thicknesses of each sample to confirm the growth rate (always in the 1.3–1.6 nm min^{-1} range). Rocking curves in ω were collected in a triple-axis configuration using a 220 Ge analyzer crystal. The surface morphology was examined by atomic force microscopy (AFM) using a Cypher ES atomic force microscope (Asylum Research) equipped with an FS-1500 Au coated Si-tip (Oxford Instruments).

The final feedback for electrical quality of the La-doped $BaSnO_3$ films was obtained using a Nanometrics HL5500 Hall system, with indium (99.9999% purity, Alfa Aesar) contacts soldered onto the edges of the sample in van der Pauw geometry.[48] The electron density was estimated by considering the thickness (t) of the La-doped $BaSnO_3$ layer (top layer). This thickness is the fraction of the growth time of the channel layer that the lanthanum shutter was open multiplied by the total thickness of the $BaSnO_3$ channel measured by XRR. The bulk carrier concentration (n) is then calculated from the measured sheet carrier concentration (n_s) of the grown film by n_s/t, where n_s is measured by using the Hall effect. Temperature-dependent Hall measurements were recorded using a Quantum Design 9T physical properties measurement system with a ±1 T field sweep for Hall measurements. Secondary ion mass spectroscopy (SIMS) was conducted by Eurofins EAG Laboratories to determine the percentage of electrically active lanthanum dopant. To perform this analysis, a 300 nm thick UID $BaSnO_3$ standard was prepared on (100) $SrTiO_3$ and implanted with $^{139}La^+$ by CuttingEdge Ions following the method outlined in Truttmann *et al.*[49] for the implantation of lanthanum in $SrSnO_3$. In particular, an implantation energy of 175 keV and dose of 2.07×10^{14} cm^{-2} at a 7° tilt angle was used to avoid channeling in the standard.

Structural analysis of one of the best samples (possessing a high μ at a low n_s) was done using cross-sectional scanning transmission electron microscopy (STEM). The TEM specimen was prepared using a focused-ion beam following standard lift-out procedures. The samples were thinned to electron transparency, with the Ga beam energy decreasing from 30 to 2 kV. High-angle annular dark-field (HAADF) STEM images were acquired using an aberration-corrected STEM [Thermo Fisher Scientific Spectra 200 (S)TEM] equipped with probe aberration corrector, operated at 200 kV. Energy dispersive x-ray (EDX) spectroscopy data were collected using the Spectra 200 microscope with a dual-x detector.

RESULTS AND DISCUSSION

La-doped $BaSnO_3$ films[4,6,7,9,11,44] and single crystals[1] with the highest mobility from the literature, as well as more recent films grown on a selection of perovskite substrates [(100) $LaAlO_3$ and (100) $SrTiO_3$] and (100) MgO using the conditions described in Ref. 6, are plotted in Fig. 1(a) as functions of their carrier concentration. The highest mobility of these films is 194 cm^2 V^{-1} s^{-1}, with a sheet carrier density of 1.6×10^{15} cm^{-2} at room temperature. This record-mobility film had a channel layer (t) of La-doped $BaSnO_3$ grown to a thickness of 70 nm on a (100) $LaAlO_3$ substrate with a 140 nm thick UID $BaSnO_3$ buffer layer. This corresponds to an electron concentration of 2.2×10^{20} cm^{-3} in the layer. Characterization of this sample by XRD and temperature-dependent Hall effect is presented in Figs. S13 and S14 of the supplementary material. An analysis of the temperature-dependent Hall data is

08 November 2026 01:46:08

© Author(s) 2026

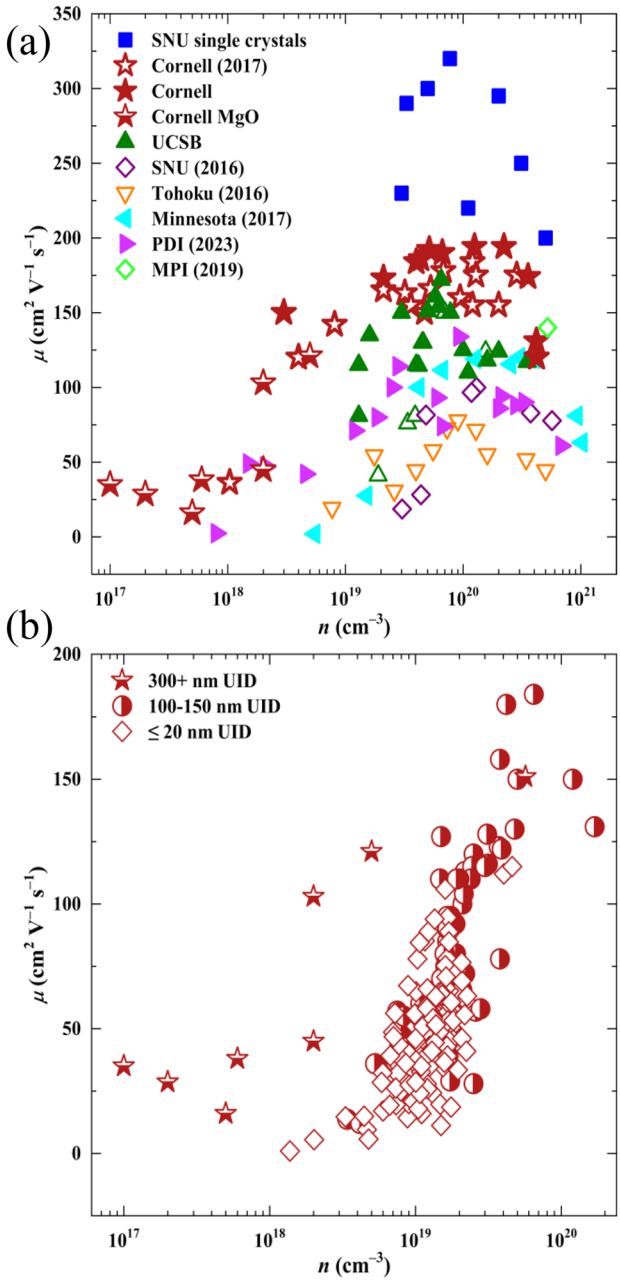


FIG. 1. (a) Comparison of the reported mobility of La-doped $BaSnO_3$ films [the filled red stars represent Cornell (this work); the open red stars denote Cornell (2017) Ref. 6; the filled green upward pointing triangles denote UCSB Ref. 44; the open purple diamonds represent SNU (2016) Ref. 25; the down pointing orange triangles represent Tohoku (2016) Ref. 35; the teal filled left pointing triangles represent Minnesota (2017) Ref. 7; the right pointing filled purple triangles represent PDI (2023) Ref. 11; and the green hollow diamond represents MPI (2019) Ref. 8] and single crystals [the blue filled squares represent SNU (2012) Refs. 1 and 2] as a function of mobile electron carrier concentration (n) at room temperature. (b) The same comparison, but for La-doped $BaSnO_3$ films grown on (100) MgO substrates with ~300+ nm thick UID buffer layers (red half-filled stars), 100–150 nm thick UID buffer layers (half-filled red circles represent the work from Ref. 10), and with ≤20 nm buffer layers (open red diamonds).

found in Fig. S15, wherein we consider the possible scattering mechanisms limiting the electron mobility in this highest mobility sample.

From Fig. 1(a) it is evident that the peak in mobility for La-doped $BaSnO_3$ thin films occurs near carrier concentrations of ~(1–2) × 10^{20} cm^{-3}. This peak in thin-film mobility is far below the highest observed mobilities in La-doped $BaSnO_3$ single crystals at comparable doping, where mobilities as high as 320 cm^2 V^{-1} s^{-1} have been demonstrated.[1] Common to both single crystals and thin films of La-doped $BaSnO_3$ is a decline in mobility with decreasing carrier concentration below about 1 × 10^{20} cm^{-3}. A sharp decline in mobility of single-crystal La-doped $BaSnO_3$ is observed, with no conducting samples below 1 × 10^{19} cm^{-3}, as denoted by the blue squares shown in Fig. 1(a). This trend is similar for thin films, although we have been able to grow conducting samples with low mobilities at carrier densities as low as 1 × 10^{17} cm^{-3}.

All the films shown in Fig. 1(a) contain a 10–330 nm thick UID $BaSnO_3$ layer between the conducting La-doped $BaSnO_3$ channel and underlying substrate. Functionally, the introduction of a UID buffer layer works to lower the density of threading dislocations in the conducting channel and provide an interface with conceivably less scattering to flowing electrons (the UID $BaSnO_3$/La-doped $BaSnO_3$ interface compared with the MgO/La-doped $BaSnO_3$ interface). While these channel properties are attractive for $BaSnO_3$-based transistors, modern ribbonFET or finFET designs necessitate thin structures to physically fit and, therefore, impose a thickness budget on the channel layer.[50] Furthermore, it is desired to only have conductivity in the La-doped $BaSnO_3$ channel and avoid parasitic leakage in the substrate or UID buffer layer. Such leakage could arise from many potential sources, including persistent photoconductivity in UID $BaSnO_3$[51] or conductivity on the surface of an underlying substrate such as $SrTiO_3$ after it has been Ar-ion etched.[52] These concerns make it desired to have minimal or even no UID $BaSnO_3$ and to utilize a substrate that is robust against processing steps. For this reason, we limit our study to the growth of La-doped $BaSnO_3$ on thin UID $BaSnO_3$ or directly on (100) MgO substrates, a robustly insulating substrate with a bandgap of about 7.5 eV.[53,54]

Figure 1(b) shows μ vs n achieved in La-doped $BaSnO_3$ films grown on (100) MgO with and without thick (100–330 nm) UID $BaSnO_3$ buffer layers. The mobility of the La-doped $BaSnO_3$ films is clearly lower without the thick UID $BaSnO_3$ buffer layers, especially at low doping. Nonetheless, to remove potential unwanted leakage and remain within the thickness limitations of modern transistor designs, we focus on establishing the Hall effect mobility that can be achieved in thin La-doped $BaSnO_3$ on (100) MgO substrates with and without thin UID $BaSnO_3$ buffer layers ≤20 nm.

A theoretical description of n-type carrier mobility in a dislocation-limited crystal, i.e., a transistor channel, can be found in the work of Podor *et al.*[37] wherein μ is deduced to depend on the square root of n, i.e., $\mu \propto \sqrt{n}$. As this bulk carrier concentration is equal to n_s divided by t, $n = \frac{n_s}{t}$, we can rewrite Podor's equation as $\mu \propto \sqrt{\frac{n_s}{t}}$. Following this equation, to increase the mobility of a channel material riddled by threading dislocations, one can lower t or raise n_s. The need to fully deplete the channel and achieve a good on/off ratio of the current passing through the transistor puts an upper limit on n_s, $n_{s,\max}$, which depends on the gate dielectric used. Podor's equation then becomes $\mu \propto \sqrt{\frac{n_{s,\ \max}}{t}}$, where $n_{s,\ \max}$ is

08 November 2026 01:46:08

© Author(s) 2026

a fixed value. This equation implies that the mobility will be maximized when the conducting channel is as thin as possible. A thin channel must be highly doped to contain $n_{s,\max}$. Recognizing from Fig. 1(a) that the mobility of La-doped $BaSnO_3$ plummets at carrier concentrations higher than about 2×10^{20} cm^{-3} led us to initially study the mobility of ultra-thin, highly doped La-doped $BaSnO_3$ channels in an attempt to maximize the channel mobility without a UID $BaSnO_3$ buffer layer.

Following this ultra-thin, highly doped channel strategy led to the results shown in Fig. S1 of the supplementary material, where it is evident that conducting films of La-doped $BaSnO_3$ are achievable down to channel thicknesses of 5 nm at constant n [(8–9) $\times 10^{19}$ cm^{-3}]. Unfortunately, the mobility is seen to fall below 50 cm^2 V^{-1} s^{-1} for sheet carrier densities less than 8×10^{13} cm^{-2}. This is disappointing due to the low mobility measured at such a high carrier concentration compared to what is needed to be able to pinch off a transistor by most gate dielectrics, e.g., n_s must be less than 5×10^{13} cm^{-2} for an HfO_2 dielectric. We abandon this strategy in favor of thicker La-doped $BaSnO_3$ films that are more lightly doped, which we show in the following to provide higher mobility at lower sheet carrier densities than this initial approach. Possible explanations of why our initial approach of minimizing channel thickness is flawed are (1) the TDD is not constant (it decreases with film thickness), (2) there is a significant concentration of traps at the MgO/La-doped $BaSnO_3$ interface, and (3) our approach ignores interface scattering, which increases as the La-doped $BaSnO_3$ channel is reduced in thickness. A low doping approach with thicker films was found to work better to realize device-relevant La-doped $BaSnO_3$ channels, as described next.

Figure 2 shows mobility as a function of the sheet carrier density of 209 La-doped $BaSnO_3$ films grown under different conditions. A comparison of three SnO:Ba flux ratios investigated in this work are plotted in Fig. 2 along with prior La-doped $BaSnO_3$ films. From the plot, it is evident that increasing the SnO:Ba flux ratio leads to slightly improved mobilities at similar sheet carrier concentrations. Films grown with a 4:1 ratio of SnO:Ba exhibit high mobilities most reproducibly, and in contrast, films grown with a 1.2:1 ratio of SnO:Ba demonstrate less reproducible electronic properties. While both conditions imply growth in an adsorption-controlled window where excess SnO is supplied, the higher overpressure of SnO in the 4:1 ratio films could be decreasing V_{Sn}'''' point defects[42] or $(BaO)_2$ crystallographic shear defects,[45] leading to the greater consistency of high mobility. Other studies suggest that increased SnO fluxes will compensate for V_{Ba}'' that are acting as negatively charged scattering sites for mobile carriers by accommodating Sn_{Ba} anti-site point defects.[44] These sites would, in theory, be neutrally charged due to the Sn^{2+} valence state. The size of these ions (Sn^{2+} and Ba^{2+}) are comparable: 12-coordinated Ba^{2+} has a coordination radius of 1.75 Å,[55] whereas 12-coordinated Sn^{2+} has a coordination radius of 1.32 Å.[56] We find such anti-site defects unlikely, however, as it has proven relatively difficult to achieve the Sn^{2+} oxidation state, especially in perovskite structures.[57–60]

The optimization of the electrical properties of La-doped $BaSnO_3$ is intertwined with the oxygen environment during growth with two competing approaches possible: growth in an oxygen-rich[44] or oxygen-poor[42] environment. In our study, we found oxygen-poor conditions during growth and after growth (by vacuum cooling samples from growth temperature to below 200 °C) to provide a higher yield of conducting samples at the low lanthanum doping that is the subject of this study. Expectedly, with increased fluxes of SnO, there is an increased partial pressure of O_2 emitting from the source material, but from our experience with the growth of Sn^{2+}-compounds (where we find it essential to avoid any ozone),[61–63] we expect our use of 10% ozone plus 90% oxygen as an oxidant at a background pressure exceeding 5×10^{-7} Torr to fully oxidize all tin to the 4+ valence state.

Although a SnO:Ba ratio of 4:1 was found to more reproducibly yield higher mobility films at the same sheet carrier concentration, the surface morphology of these films was often rough. Variations of the surface quality at this 4:1 flux ratio are seen for three films in Fig. S2 of the supplementary material. Small, broadly distributed precipitates in the case of slightly Ba-rich growth or Sn-rich

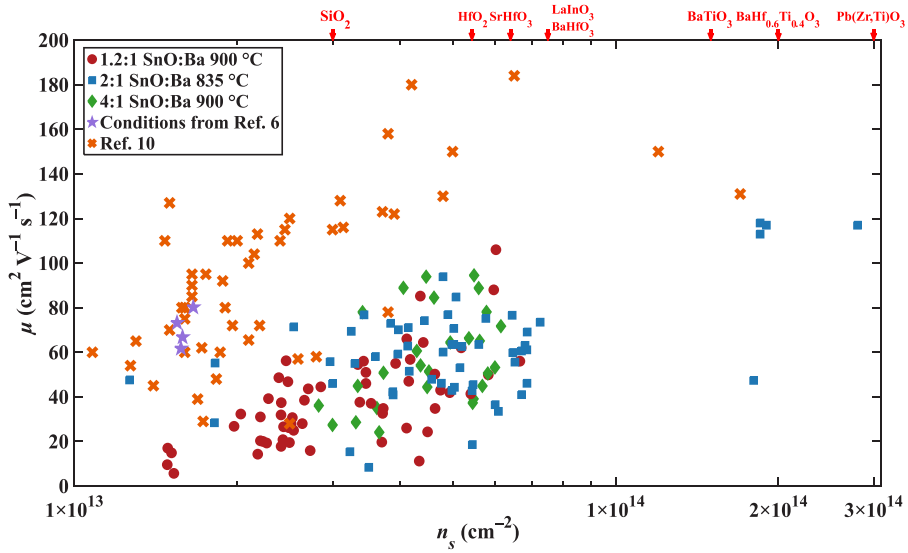


FIG. 2. Mobility vs sheet carrier density plot for samples grown with and without thick buffer layers using ozone-assisted MBE. The red arrows show a higher limit of depletion for choice gate dielectrics and ferroelectrics. The orange crosses are from Ref. 10.

08 November 2026 01:46:08

© Author(s) 2026

precipitates that are less distributed but taller are seen and, in both cases, retain reasonable mobilities. The slight non-stoichiometry of the films shown in Fig. S2 of the supplementary material was revealed by etching the films in either deionized (DI) water—to dissolve the Ba-rich [likely $Ba(OH)_2$ or $BaCaO_3$] precipitates—or a mixture of concentrated hydrochloric acid and peroxide to dissolve the Sn-rich (likely SnO_2) precipitates, as shown in Fig. S3 of the supplementary material. A higher mobility is found for the sample with no observed precipitates in a 10 × 10 μm^2 scan, and this same sample has a root mean square (rms) roughness of 0.28 nm. Notably, the RHEED patterns for all three samples look indiscernible from one another (see Fig. S2 of the supplementary material), which suggests that even the off-stoichiometric surface compositions are a small deviation from ideal.

In contrast, for the lower SnO:Ba ratio of 1.2:1 more variance in mobility is seen, shown in Fig. 2. Nevertheless, these films are reproducibly smoother and lack the significant variation in surface morphology as was the case for the 4:1 ratio, with a comparison shown in Fig. S4 of the supplementary material. The ratio of 2:1 for SnO:Ba was found to produce the greatest yield of conducting La-doped $BaSnO_3$ samples in thin layers at the low doping concentrations studied, lowering the substrate temperature functions to increase the sticking coefficient of the volatile SnO species on the surface of the substrate. Simultaneously, a reduced SnO flux is used to remain in the adsorption-controlled regime and avoid the accumulation of excess SnO_2 on the film during growth. Utilizing these growth controls, we attempt to target minimal variation in surface roughness and correspondingly smaller variation in mobility.

Focusing on samples that have a total thickness of less than 40 nm and doping less than 2 × 10^{19} cm^{-3} shows that mobilities of up to 106 cm^2 V^{-1} s^{-1} are achievable. As illustrated in Fig. 3(a), this mobility is reduced as the conducting channel layer gets thinner

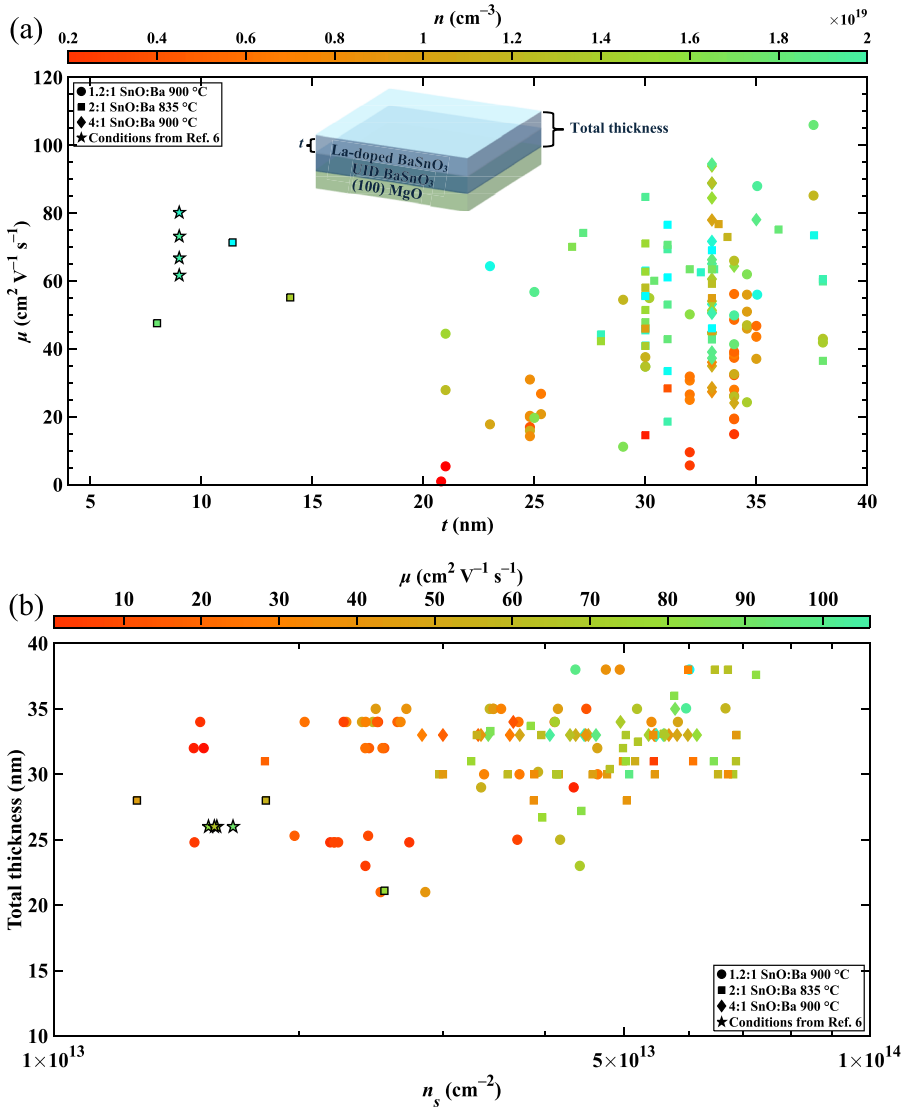


FIG. 3. (a) Mobility vs channel layer thickness plot for La-doped $BaSnO_3$ films with ≤20 nm of UID $BaSnO_3$ between the channel layer and (100) MgO substrate. The filled stars are samples grown using the conditions from Ref. 6 with a 17 nm thick UID $BaSnO_3$ buffer layer. The inset illustrates an example structure containing both UID $BaSnO_3$ and La-doped $BaSnO_3$ grown on MgO (100). (b) A plot of total thickness vs sheet carrier concentration for the same sample set shown in panel (a). The data points with the black outlines have a UID $BaSnO_3$ buffer layer (~20 nm thick); those without a black outline have ≤1 U.C. UID $BaSnO_3$ buffer layer.

08 November 2026 01:46:08

© Author(s) 2026

with no UID $BaSnO_3$ layer present. Indeed, this agrees with prior observations of highly lattice-mismatched semiconducting systems such as InAs on GaAs,[64] InSb on GaAs,[40] germanium on silicon,[65] and GaN on Al_2O_3.[39] Figure 3(a) also shows thin La-doped $BaSnO_3$ channels (stars) grown using the conditions of Paik *et al.*[6] that demonstrate high mobilities at channel thicknesses <10 nm with sheet carrier densities of ~2×10^{13} cm^{-2}; an example schematic of this structure is displayed as an inset in Fig. 3(a). Viewing these samples by total thickness represented in Fig. 3(b) clarifies that thin channels with desirable electrical properties have a comparable total thickness (yet another alternative view is shown in the supplementary material, Fig. S5). Using this concept, a 2:1 ratio film was grown to a total thickness of ~21 nm with a ~10 nm La-doped $BaSnO_3$ channel that exhibited a sheet carrier density of 2.5×10^{13} cm^{-2} with a mobility of 71 cm^2 V^{-1} s^{-1}.

An alternative view of the same data displayed in Fig. 2 is presented in Fig. 4, where instead of plotting sheet carrier density vs mobility, we have an engineering plot illustrating the competition among La-doped $BaSnO_3$ channel thickness, carrier concentration, and mobility. This representation shows the available paths to optimizing the conducting channel for a specified device structure. However, considering sheet carrier densities by multiplying the thickness of the conducting channel by its carrier concentration can clarify the electric field needed to deplete the channel. It then becomes straightforward to consider the product of $\kappa \times E_{BD}$ for a gate dielectric or the P_s of a ferroelectric and determine the higher limit of depletable channels. Ideally, achieving the lowest product of $t \times n$ is preferred to allow for complete pinch off based on the choice of transistor structure. The red arrows illustrated in Fig. 2 represent a higher limit of depletion achievable for some potential gate dielectrics and ferroelectrics. In the process of minimizing the sheet carrier density (represented by the dashed lines shown in Fig. 4), the 4:1 SnO:Ba ratio still demonstrates the highest mobilities with reproducibility at sheet carrier densities of (4–5) $\times 10^{13}$ cm^{-2}, for samples grown without a UID buffer layer.

A closer examination of the best sample grown with the 4:1 SnO:Ba ratio is captured in Fig. S6. The sharp streaks seen during growth in the RHEED pattern in Figs. S6(a) and S6(b) are consistent with a smooth surface and cube-on-cube epitaxy between the (100) La-doped $BaSnO_3$ film and (100) MgO substrate. This is corroborated by the *ex-situ* AFM scan shown in Fig. S6(c) revealing a smooth surface devoid of precipitates and is consistent with other reported films of La-doped $BaSnO_3$ with good electrical properties.[11] The film shown in Fig. S6 had no UID $BaSnO_3$ buffer layer, exhibited a room-temperature mobility of 95 cm^2 V^{-1} s^{-1}, and a sheet carrier concentration of ~5.5×10^{13} cm^{-2} (thickness of 33 nm,

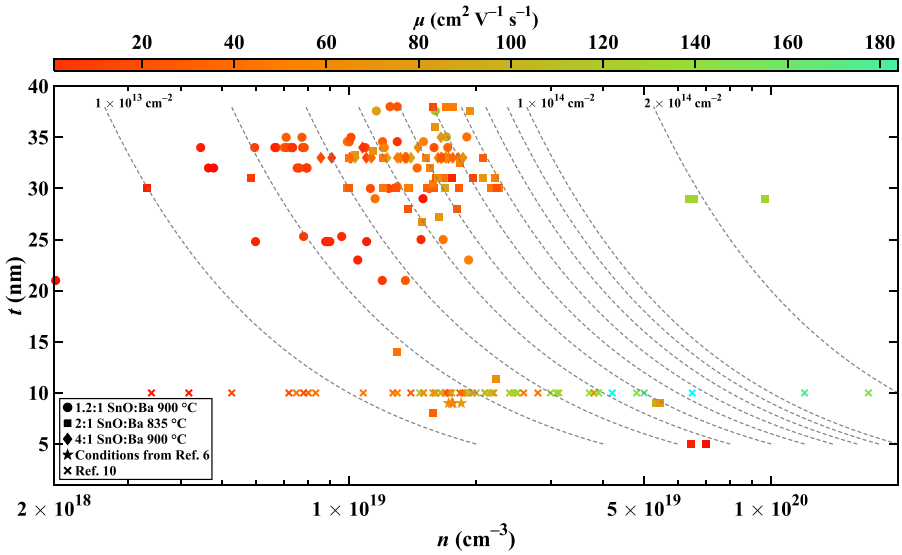


FIG. 4. Engineering plot showing the optimized parameter zone for La-doped $BaSnO_3$ grown on (100) MgO substrates from the same sample set shown in Fig. 2. Competition among thickness, mobility, and carrier concentration are illustrated by the challenges of obtaining low sheet carrier densities with high mobilities in thin, depletable layers. Different ratios of SnO to barium or growth conditions are represented by differently shaped markers (crosses represent the work from Ref. 10; the stars represent films grown using the conditions from Ref. 6).

TABLE I. Comparison of the electrical properties of five La-doped $BaSnO_3$ samples grown using different ratios of SnO:Ba with their corresponding percentage of electrically active lanthanum.

Sample ID	Ratio (SnO:Ba)	t (nm)	μ (cm^2 V^{-1} s^{-1})	n (cm^{-3})	La concentration (cm^{-3})	% La activated
Sample A	1.2:1	38	41.9	1.3×10^{19}	3.2×10^{19}	40.6
Sample B	1.2:1	38	106	1.6×10^{19}	3.7×10^{19}	43.2
Sample C	2:1	30	71.1	1.4×10^{19}	3.4×10^{19}	41.2
Sample D	2:1	30	84.8	1.7×10^{19}	2.8×10^{19}	60.7
Sample E	4:1	33	94.5	1.7×10^{19}	2.5×10^{19}	68

08 November 2026 01:46:08

© Author(s) 2026

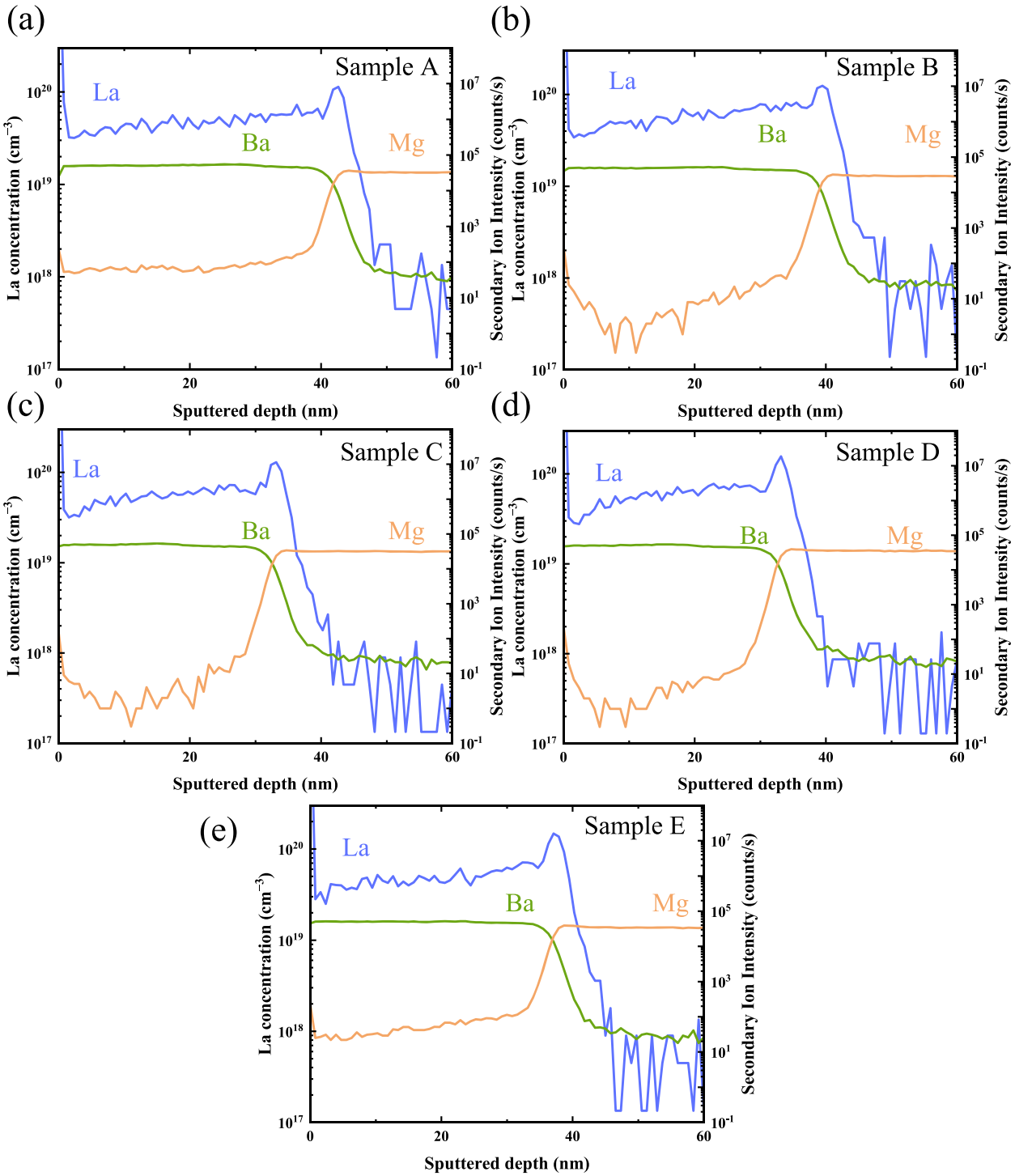


FIG. 5. SIMS of five La-doped $BaSnO_3$ thin films grown using different ratios of SnO:Ba. Panel (a) shows the SIMS measured for sample A (μ = 106 cm^2 V^{-1} s^{-1}, t = 38 nm, and $n = 1.6 \times 10^{19}$ cm^{-3}), which was grown using the 1.2:1 SnO:Ba ratio and (b) Sample B (μ = 41.9 cm^2 V^{-1} s^{-1}, t = 38 nm, $n = 1.3 \times 10^{19}$ cm^{-3}) is also shown grown with the same 1.2:1 SnO:Ba ratio. Panels (c)–(d) show the SIMS results for sample C (μ = 71.1 cm^2 V^{-1} s^{-1}, t = 30 nm, and $n = 1.38 \times 10^{19}$ cm^{-3}) and sample D (μ = 84.8 cm^2 V^{-1} s^{-1}, t = 30 nm, and $n = 1.69 \times 10^{19}$ cm^{-3}), respectively, and were both grown using the 2:1 ratio of SnO:Ba. Panel (e) represents the 4:1 SnO:Ba ratio case, with sample E (μ = 94.5 cm^2 V^{-1} s^{-1}, t = 33 nm, and $n = 1.66 \times 10^{19}$ cm^{-3}) being a better performing sample.

08 November 2026 01:46:08

© Author(s) 2026

carrier concentration of 1.7×10^{19} cm^{-3}). To quantify the structural quality of the La-doped $BaSnO_3$ film, a rocking curve in ω of the 200 La-doped $BaSnO_3$ peak is overlaid onto the 200 MgO substrate peak shown in Fig. S6(e). The full width at half maximum (FWHM) in ω of the MgO substrate is found to be 54 arc sec, and the La-doped $BaSnO_3$ film grown on top has a FWHM of 72 arc sec. It is common for (100) MgO substrates to have such poor crystallinity[66] compared to higher-quality oxide substrates that are grown by using the Czochralski method[67] and through epitaxy this reduced crystallinity is translated into the film.

The out-of-plane lattice constant (a_{oop}) for the same film shown in Fig. S6 was determined using a Nelson–Riley fit[68] and found to be 4.102 ± 0.001 Å. Following the suggestion that La-doped $BaSnO_3$ films with larger a_{oop} have higher mobility,[44] we measured a_{oop} of many of our La-doped $BaSnO_3$ films grown on (100) MgO. As is evident from Fig. S7, we do not observe this correlation; there are many films with low or no mobility at similar a_{oop} to those with high mobility. The samples included within Fig. S6 have varying lanthanum content and it is possible that the change of doping concentration also influences a_{oop} of the film to some extent. The wide variation of electrical properties seen in films with similar a_{oop} suggests that other influences, such as crystal quality, TDD, and the presence of RP defects, make it challenging to determine whether a film has a high mobility based solely on the value of a_{oop} for the growth conditions we are using.

At a low sheet carrier density of 3.4×10^{13} cm^{-2}, there are two standout films with no buffer layer and nearly identical mobilities: 77–78 cm^2 V^{-1} s^{-1}. They are grown at SnO:Ba ratios of 2:1 and 4:1, respectively. The film grown at the 2:1 SnO:Ba ratio is the focus of Fig. S8. The structural quality seen at the surface by RHEED is comparable with the 4:1 film, as shown in Figs. S8(a) and S8(b). Sharp streaks and visible Kikuchi lines[69] are seen in both Figs. S8(a) and S8(b). In addition, an examination of the structural perfection of the film is illustrated in Fig. S8(d), where a rocking curve in ω of the 200 La-doped $BaSnO_3$ peak (FWHM of 1656 arc sec) is overlapping the respective 200 MgO substrate peak (FWHM of 101 arc sec). A linear scale normalized rocking curve for the films shown in Figs. S6 and S8 are shown in Fig. S9. In Fig. S8(c), we see a zoomed-in θ–2θ XRD scan centered on the 200 peaks of the film and substrate without the presence of any SnO_2 impurity peaks. An AFM scan of the surface, Fig. S8(e), reveals a rms roughness <0.25 nm, which is smoother than that seen in the 4:1 ratio case.

Figure S8(f) shows a drift-corrected cross-sectional HAADF-STEM image of the same sample in a region with both a threading dislocation and a Ruddlesden–Popper (RP) crystallographic shear fault present. Based on STEM images taken of this sample at lower magnification, the TDD was estimated to be (6–10) × 10^{10} cm^{-2}. While this TDD is higher than previously reported samples of La-doped $BaSnO_3$ grown by MBE,[6] the observed TDD is not surprising given the choice of substrate, (100) MgO. The density of RP defects in the crystal was determined to be ~1 × 10^{10} cm^{-2}. This density of RP defects is an order of magnitude higher than previously grown La-doped $BaSnO_3$ with thick UID $BaSnO_3$ buffer layers on (110) $DyScO_3$,[6] suggesting RP defects as a potential limiting factor for achieving high mobility in thin layers. More STEM images are included in Figs. S10–S12 of the supplementary material, which show an otherwise homogeneous film.

SIMS measurements were performed on a selection of La-doped $BaSnO_3$ thin films from each SnO:Ba ratio to examine the fraction of electrically active lanthanum dopants in each sample. By comparing the total number of lanthanum ions measured by SIMS against the concentration of free electrons n measured using Hall, we obtain the percentage of electrically active lanthanum in the films, with the results presented in Table I. From the comparison, we see that 40%–68% of the lanthanum dopants are electrically active, with the highest free carrier fractions achieved in the 2:1 and 4:1 SnO:Ba case. One explanation for this is that the increased overpressure of SnO lowers the number of trap states that develop during the growth—possibly V''''_{Sn} point defects. Figures 5(a)–5(e) show the SIMS profiles of the selected La-doped $BaSnO_3$ thin films, with a clear slope in the lanthanum concentration observed in each SnO:Ba ratio case. SIMS artifacts are observed at both interfaces of the La-doped $BaSnO_3$ thin film due to the film surface and the change in matrix from $BaSnO_3$ to MgO and can be ignored. An increasing lanthanum concentration with depth is evident in all of the films. In contrast, a flat lanthanum concentration is seen in SIMS profiles of La-doped $BaSnO_3$ grown on the lattice-matched substrate (100) Ba_2ScNbO_6[70] using analogous growth conditions with 100% dopant activation,[71] making us suspect that the observed lanthanum gradient is due to the high concentration of threading dislocations in the La-doped $BaSnO_3$ films grown on (100) MgO for this study. Threading dislocations could conceivably impact the diffusion of the lanthanum dopant by providing a fast diffusion path to the sample surface for the dopant. Indeed, the observation of lanthanum segregation in La-doped $BaSnO_3$ has been noted by EDX and STEM in the work of Yun *et al.*[72] with the presence of lanthanum anti-site occupancy in the core of threading dislocations and an increase in the presence of Sn-terminated half planes.

CONCLUSION

Our results show that using *S*-MBE while employing a narrow adsorption-controlled growth window allows for the synthesis of thin, high mobility layers of La-doped $BaSnO_3$ directly onto (100) MgO substrates. By introducing a UID $BaSnO_3$ buffer layer with a thickness of about 10–20 nm, the growth of La-doped $BaSnO_3$ with low sheet carrier densities of (1–3) × 10^{13} cm^{-2} is possible. One such exemplary buffer layer sample retained a reasonably high mobility of 71 cm^2 V^{-1} s^{-1} at a sheet carrier density of 2.5×10^{13} cm^{-2}. Our study shows that La-doped $BaSnO_3$ channels directly deposited on MgO can have mobilities of 77–78 cm^2 V^{-1} s^{-1} at a sheet carrier density of 3.4×10^{13} cm^{-2} and 95 cm^2 V^{-1} s^{-1} at a sheet carrier density of 5.5×10^{13} cm^{-2}. When considered as the channel layer of a transistor, such sheet carrier densities should be depletable, depending on the choice of gate dielectric or ferroelectric. Conductive films with n_s as low as 1×10^{13} cm^{-2} were achieved when directly deposited on MgO substrates, but with barely two-digit mobilities. Striving for these electrical properties in thin films, on the order of 10 nm or less, is critical to moving toward the requirements of a next generation ribbonFET or finFET design for industrial manufacturing. A trend of increasing mobility with sheet carrier concentration was seen for samples with $n_s < 2 \times 10^{14}$ cm^{-2}, which is typical of La-doped $BaSnO_3$,[1,6,10,23,34] although our study extends this to record-low n_s for films with no UID buffer layer. SIMS measurements of a few

08 November 2026 01:46:08

© Author(s) 2026

La-doped $BaSnO_3$ films from each SnO:Ba ratio examined in this study reveal 40%–68% electrically activated lanthanum, with the 2:1 and 4:1 ratio conditions improving the free carrier fraction. The sheet carrier densities of our best films remain in the degenerately doped regime but are expected to be depletable given the proper selection of materials for oxide perovskite transistors.

SUPPLEMENTARY MATERIAL

The supplementary material provides additional characterization, STEM images, and temperature-dependent Hall data on the highest mobility La-doped $BaSnO_3$ thin film.

ACKNOWLEDGMENTS

The synthesis work at Cornell (N.A.P., S.L., and D.G.S.) was supported by Intel Corporation and the National Science Foundation through the AI Research Institutes program Award No. DMR-2433348. J.R.W. and D.A.T. acknowledge support from the National Science Foundation (Grant No. DMR-2104918). The authors thank Steven Button for facilitating substrate preparation.

AUTHOR DECLARATIONS

Conflict of Interest

The authors have no conflicts to disclose.

Author Contributions

Nicholas A. Parker: Conceptualization (equal); Data curation (equal); Formal analysis (equal); Investigation (equal); Methodology (equal); Visualization (equal); Writing – original draft (equal); Writing – review & editing (equal). **Seungmin Lee**: Conceptualization (equal); Data curation (equal); Formal analysis (equal); Investigation (equal); Methodology (equal); Writing – review & editing (equal). **Adedapo Oni**: Data curation (equal); Formal analysis (equal); Investigation (equal); Writing – original draft (supporting). **George N. Kotsonis**: Data curation (supporting); Formal analysis (supporting); Investigation (supporting); Methodology (supporting). **Kathy Azizie**: Data curation (supporting); Investigation (supporting); Validation (supporting); Writing – review & editing (supporting). **Jisung Park**: Data curation (equal); Formal analysis (equal); Investigation (equal). **Hanjong Paik**: Data curation (equal); Formal analysis (equal); Investigation (equal). **Jacary Sapp**: Data curation (supporting); Investigation (supporting). **Jay R. Wright**: Data curation (supporting); Investigation (supporting). **D. Jena**: Funding acquisition (lead); Resources (supporting). **H. G. Xing**: Funding acquisition (lead); Resources (supporting). **Dmitri A. Tenne**: Funding acquisition (lead). **Punyashloka Debashis**: Conceptualization (equal); Funding acquisition (supporting); Methodology (equal). **Pratyush Buragohain**: Conceptualization (equal); Funding acquisition (supporting); Investigation (equal); Methodology (equal); Writing – review & editing (equal). **Raseong Kim**: Conceptualization (equal); Funding acquisition (supporting); Methodology (equal); Writing – review & editing (equal). **Rachel Steinhardt**: Conceptualization (equal); Funding acquisition (equal); Investigation (equal); Methodology (equal); Project administration (supporting); Resources (supporting); Writing – review & editing (equal). **Darrell G. Schlom**: Conceptualization (equal); Formal analysis (equal); Funding acquisition (equal); Investigation (equal); Methodology (equal); Project administration (equal); Resources (equal); Writing – original draft (equal); Writing – review & editing (equal).

DATA AVAILABILITY

The data that support the findings of this study are available within the article. Additional data related to the growth and structural characterization are available at https://www.doi.org/10.5281/zenodo.23348710. Any additional data connected to the study are available from the corresponding author upon reasonable request.

REFERENCES

[1] H. J. Kim, U. Kim, H. M. Kim, T. H. Kim, H. S. Mun, B.-G. Jeon, K. T. Hong, W.-J. Lee, C. Ju, K. H. Kim, and K. Char, Appl. Phys. Express **5**, 061102 (2012).
[2] H. J. Kim, U. Kim, T. H. Kim, J. Kim, H. M. Kim, B.-G. Jeon, W.-J. Lee, H. S. Mun, K. T. Hong, J. Yu, K. Char, and K. H. Kim, "Physical properties of transparent perovskite oxides (Ba,La)SnO_3 with high electrical mobility at room temperature," Phys. Rev. B **86**(16), 165205 (2012).
[3] X. Luo, Y. S. Oh, A. Sirenko, P. Gao, T. A. Tyson, K. Char, and S. W. Cheong, "High carrier mobility in transparent $Ba_{1-x}La_xSnO_3$ crystals with a wide band gap," Appl. Phys. Lett. **100**(17), 172112 (2012).
[4] S. Raghavan, T. Schumann, H. Kim, J. Y. Zhang, T. A. Cain, and S. Stemmer, "High-mobility $BaSnO_3$ grown by oxide molecular beam epitaxy," APL Mater. **4**, 016106 (2016).
[5] Z. Galazka, R. Uecker, K. Irmscher, D. Klimm, R. Bertram, A. Kwasniewski, M. Naumann, R. Schewski, M. Pietsch, U. Juda, A. Fiedler, M. Albrecht, S. Ganschow, T. Markurt, C. Guguschev, and M. Bickermann, "Melt growth and properties of bulk $BaSnO_3$ single crystals," J. Phys.: Condens. Matter **29**, 075701 (2017).
[6] H. Paik, Z. Chen, E. Lochocki, A. Seidner H, A. Verma, N. Tanen, J. Park, M. Uchida, S. Shang, B.-C. Zhou, M. Brützam, R. Uecker, Z.-K. Liu, D. Jena, K. M. Shen, D. A. Muller, and D. G. Schlom, "Adsorption-controlled growth of La-doped $BaSnO_3$ by molecular-beam epitaxy," APL Mater. **5**, 116107 (2017).
[7] A. Prakash, P. Xu, A. Faghaninia, S. Shukla, J. W. Ager, C. S. Lo, and B. Jalan, "Wide bandgap $BaSnO_3$ films with room temperature conductivity exceeding 10^4 S cm^{-1}," Nat. Commun. **8**, 15167 (2017).
[8] A. P. Nono Tchiomo, W. Braun, B. P. Doyle, W. Sigle, P. van Aken, J. Mannhart, and P. Ngabonziza, "High-temperature-grown buffer layer boosts electron mobility in epitaxial La-doped $BaSnO_3/SrZrO_3$ heterostructures," APL Mater. **7**(4), 041119 (2019).
[9] W. M. Postiglione, K. Ganguly, H. Yun, J. S. Jeong, A. Jacobson, L. Borgeson, B. Jalan, K. A. Mkhoyan, and C. Leighton, "Structure-property relationships and mobility optimization in sputtered La-doped $BaSnO_3$ films: Toward 100 cm^2 V^{-1} s^{-1}," Phys. Rev. Mater. **5**(4), 044604 (2021).
[10] J. Park, H. Paik, K. Nomoto, K. Lee, B. E. Park, B. Grisafe, L. C. Wang, S. Salahuddin, S. Datta, Y. Kim, D. Jena, H. G. Xing, and D. G. Schlom, "Fully transparent field-effect transistor with high drain current and on-off ratio," APL Mater. **8**(1), 011110 (2020).
[11] G. Hoffmann, "Polarization-discontinuity-doped two-dimensional electron gas in $BaSnO_3/LaInO_3$ heterostructures grown by plasma-assisted molecular beam epitaxy," Ph.D. thesis, Humboldt-Universitat zu Berlin, 2022, p. 82.
[12] B. Ostrick, M. Fleischer, and H. Meixner, "High-temperature hall measurements on $BaSnO_3$ ceramics," J. Am. Ceram. Soc. **80**(8), 2153–2156 (1997).
[13] H. Mizoguchi, H. W. Eng, and P. M. Woodward, "Probing the electronic structures of ternary perovskite and pyrochlore oxides containing Sn^{4+} or Sb^{5+}," Inorg. Chem. **43**, 1667–1680 (2004).

08 November 2026 01:46:08

© Author(s) 2026

[14]W. Aggoune, A. Eljarrat, D. Nabok, K. Irmscher, M. Zupancic, Z. Galazka, M. Albrecht, C. Koch, and C. Draxl, "A consistent picture of excitations in cubic $BaSnO_3$ revealed by combining theory and experiment," Commun. Mater. **3**(1), 12 (2022).
[15]U. Kim, "$BaSnO_3$: Thin film growth, transport properties, devices, and interfaces," Ph.D. thesis, Seoul National University, 2015, p. 15.
[16]W.-J. Lee, H. J. Kim, J. Kang, D. H. Jang, T. H. Kim, J. H. Lee, and K. H. Kim, "Transparent perovskite barium stannate with high electron mobility and thermal stability," Annu. Rev. Mater. Res. **47**(1), 391–423 (2017).
[17]A. Ohtomo and A. Tsukazaki, "Pulsed laser deposition of thin films and superlattices based on ZnO," Semicond. Sci. Technol. **20**(4), S1–S12 (2005).
[18]Z. Galazka, K. Irmscher, M. Pietsch, S. Ganschow, D. Schulz, D. Klimm, I. M. Hanke, T. Schroeder, and M. Bickermann, "Experimental Hall electron mobility of bulk single crystals of transparent semiconducting oxides," J. Mater. Res. **36**, 4746–4755 (2021).
[19]E. Sachet, C. T. Shelton, J. S. Harris, B. E. Gaddy, D. L. Irving, S. Curtarolo, B. F. Donovan, P. E. Hopkins, P. A. Sharma, A. L. Sharma, J. Ihlefeld, S. Franzen, and J.-P. Maria, Nat. Mater. **14**, 414–420 (2015).
[20]F. P. Koffyberg, "Thermoreflectance spectra of CdO: Band gaps and band-population effects," Phys. Rev. B **13**(10), 4470–4476 (1976).
[21]V. Venkatachalapathy, A. Galeckas, R. Sellappan, D. Chakarov, and A. Y. Kuznetsov, "Tuning light absorption by band gap engineering in ZnCdO as a function of MOVPE-synthesis conditions and annealing," J. Cryst. Growth **315**(1), 301–304 (2011).
[22]C. Park, U. Kim, C. J. Ju, J. S. Park, Y. M. Kim, and K. Char, "High mobility field effect transistor based on $BaSnO_3$ with Al_2O_3 gate oxide," Appl. Phys. Lett. **105**(20), 203503 (2014).
[23]Y. M. Kim, C. Park, U. Kim, C. Ju, and K. Char, "High-mobility $BaSnO_3$ thin-film transistor with HfO_2 gate insulator," Appl. Phys. Express **9**(1), 011201 (2015).
[24]U. Kim, C. Park, T. Ha, Y. M. Kim, N. Kim, C. Ju, J. Park, J. Yu, J. H. Kim, and K. Char, "All-perovskite transparent high mobility field effect using epitaxial $BaSnO_3$ and $LaInO_3$," APL Mater. **3**, 036101 (2015).
[25]J. Shin, Y. M. Kim, Y. Kim, C. Park, and K. Char, "High mobility $BaSnO_3$ films and field effect transistors on non-perovskite MgO substrate," Appl. Phys. Lett. **109**(26), 262102 (2016).
[26]Y. M. Kim, C. Park, T. Ha, U. Kim, N. Kim, J. Shin, Y. Kim, J. Yu, J. H. Kim, and K. Char, "High-K perovskite gate oxide $BaHfO_3$," APL Mater. **5**(1), 016104 (2017).
[27]J. Yue, A. Prakash, M. C. Robbins, S. J. Koester, and B. Jalan, "Depletion mode MOSFET using La-doped $BaSnO_3$ as a channel material," ACS Appl. Mater. Interfaces **10**, 21061–21065 (2018).
[28]J. Cheng, H. Yang, N. G. Combs, W. Wu, H. Kim, H. Chandrasekar, C. Wang, S. Rajan, S. Stemmer, and W. Lu, "Electron transport of perovskite oxide $BaSnO_3$ on (110) $DyScO_3$ substrate with channel-recess for ferroelectric field effect transistors," Appl. Phys. Lett. **118**(4), 042105 (2021).
[29]D. Song, M. Jeong, J. Kim, B. Kim, J. H. Kim, J. H. Kim, K. Lee, Y. Kim, and K. Char, "High-k perovskite gate oxide for modulation beyond 10^{14} cm^{-2}," Sci. Adv. **8**(11), eabm3962 (2022).
[30]J. Lee, J. Kim, J. Ko, and K. Char, "Micron-scale FETs of fully epitaxial perovskite oxides using chemical etching," Mater. Today Quantum **1**, 100002 (2024).
[31]H. Lee, H. Yun, B. Kim, and K. Char, "Ferroelectric switching and field effect of $Pb(Zr_{0.7}Ti_{0.3})O_3$ on $Ba_{1-x}La_xSnO_3$," Phys. Rev. Mater. **8**(8), 084402 (2024).
[32]J. Cheng, C. Wang, C. Freeze, O. Shoron, N. Combs, H. Yang, N. K. Kalarickal, Z. Xia, S. Stemmer, S. Rajan, and W. Lu, "High-current perovskite oxide $BaTiO_3/BaSnO_3$ heterostructure field effect transistors," IEEE Electron Device Lett. **41**(4), 621–624 (2020).
[33]D. E. Nikonov, C. C. Lin, U. E. Avci, T. A. Gosavi, R. Kim, I. A. Young, A. V. Penumatcha, R. Ramesh, and D. G. Schlom, "Technologies for transistors with a ferroelectric gate dielectric," U.S. Patent Application Publication US 2023/0352584 A1 (2 November 2023).
[34]H. Mun, U. Kim, H. Min Kim, C. Park, T. Hoon Kim, H. Joon Kim, K. Hoon Kim, and K. Char, "Large effects of dislocations on high mobility of epitaxial perovskite $Ba_{0.96}La_{0.04}SnO_3$ films," Appl. Phys. Lett. **102**(25), 252105 (2013).
[35]J. Shiogai, K. Nishihara, K. Sato, and A. Tsukazaki, "Improvement of electron mobility in La:$BaSnO_3$ thin films by insertion of an atomically flat insulating (Sr,Ba)SnO_3 buffer layer," AIP Adv. **6**(6), 065305 (2016).
[36]G. L. Pearson, W. T. Read, and F. J. Morin, "Dislocations in plastically deformed germanium," Phys. Rev. **93**, 666–667 (1954).
[37]B. Pödör, "Electron mobility in plastically deformed germanium," Phys. Status Solidi B **16**(2), K167–K170 (1966).
[38]L. A. Kazakevich and P. F. Lugakov, "The effect of dislocations on the charge-carrier scattering processes in silicon," Cryst. Lattice Defects Amorphous Mater. **11**(3), 179–184 (1985).
[39]H. M. Ng, D. Doppalapudi, T. D. Moustakas, N. G. Weimann, and L. F. Eastman, "The role of dislocation scattering in *n*-type GaN films," Appl. Phys. Lett. **73**(6), 821–823 (1998).
[40]X. Weng, R. S. Goldman, D. L. Partin, and J. P. Heremans, "Evolution of structural and electronic properties of highly mismatched InSb films," J. Appl. Phys. **88**(11), 6276–6286 (2000).
[41]P. Ngabonziza, J. Park, W. Sigle, P. A. van Aken, J. Mannhart, and D. G. Schlom, "Employing high-temperature-grown $SrZrO_3$ buffer to enhance the electron mobility in La:$BaSnO_3$-based heterostructures," Appl. Phys. Lett. **122**(24), 241902 (2023).
[42]L. Weston, L. Bjaalie, K. Krishnaswamy, and C. G. Van de Walle, "Origins of *n*-type doping difficulties in perovskite stannates," Phys. Rev. B **97**(5), 054112 (2018).
[43]A. Prakash and B. Jalan, "Wide bandgap perovskite oxides with high room-temperature electron mobility," Adv. Mater. Interfaces **6**(15), 1900479 (2019).
[44]N. G. Combs, W. Wu, and S. Stemmer, "Stoichiometry control in molecular beam epitaxy of $BaSnO_3$," Phys. Rev. Mater. **4**(1), 014604 (2020).
[45]W. Y. Wang, Y. L. Tang, Y. L. Zhu, J. Suriyaprakash, Y. B. Xu, Y. Liu, B. Gao, S.-W. Cheong, and X. L. Ma, "Atomic mapping of Ruddlesden-Popper faults in transparent conducting $BaSnO_3$-based thin films," Sci. Rep. **5**(1), 16097 (2015).
[46]A. V. Sanchela, M. Wei, J. Lee, G. Kim, H. Jeen, B. Feng, Y. Ikuhara, H. J. Cho, and H. Ohta, "Buffer layer-less fabrication of a high-mobility transparent oxide semiconductor, La-doped $BaSnO_3$," J. Mater. Chem. C **7**, 5797–5802 (2019).
[47]MKS Instruments, MKS ASTeX model AX8407-C3 ozone generator Data sheet (MKS Instruments, Wilmington, MA. 2018). p. 2.
[48]L. J. van der Pauw, "A method of measuring the resistivity and Hall coefficient on lamellae of arbitrary shape," Philips Tech. Rev. **20**, 220–224 (1958).
[49]T. Truttmann, A. Prakash, J. Yue, T. E. Mates, and B. Jalan, "Dopant solubility and charge compensation in La-doped $SrSnO_3$ films," Appl. Phys. Lett. **115**, 152103 (2019).
[50]D. Hisamoto, W.-C. Lee, J. Kedzierski, E. Anderson, H. Takeuchi, K. Asano, T.-J. King, J. Bokor, and C.-M. Hu, "A folded-channel MOSFET for deep-sub-tenth micron era," in *International Electron Devices Meeting 1998. Technical Digest (Cat. No. 98CH36217)* (IEEE, 1998), pp. 1032–1034.
[51]J. Park, U. Kim, and K. Char, "Photoconductivity of transparent perovskite semiconductor $BaSnO_3$ and $SrTiO_3$ epitaxial thin films," Appl. Phys. Lett. **108**(9), 092106 (2016).
[52]C. W. Schneider, S. Thiel, G. Hammerl, C. Richter, and J. Mannhart, "Microlithography of electron gases formed at interfaces in oxide heterostructures," Appl. Phys. Lett. **89**(12), 122101 (2006).
[53]D. M. Roessler and W. C. Walker, "Electronic spectrum and ultraviolet optical properties of crystalline MgO," Phys. Rev. **159**(3), 733–738 (1967).
[54]M. L. Bortz, R. H. French, D. J. Jones, R. V. Kasowski, and F. S. Ohuchi, "Temperature dependence of the electronic structure of oxides: MgO, $MgAl_2O_4$ and Al_2O_3," Phys. Scr. **41**(4), 537–541 (1990).
[55]R. D. Shannon, "Revised effective ionic radii and systematic studies of interatomic distances in halides and chalcogenides," Acta Crystallogr., Sect. A **32**(5), 751–767 (1976).
[56]V. Sidey, "On the effective ionic radii for the tin(II) cation," J. Phys. Chem. Solids **171**, 110992 (2022).
[57]M. Seth, K. Faegri, and P. Schwerdtfeger, "The stability of the oxidation state +4 in group 14 compounds from carbon to element 114," Angew. Chem., Int. Ed. **37**(18), 2493–2496 (1998).
[58]T. Fix, S.-L. Sahonta, V. Garcia, J. L. MacManus-Driscoll, and M. G. Blamire, "Structural and dielectric properties of $SnTiO_3$, a putative ferroelectric," Cryst. Growth Des. **11**(5), 1422–1426 (2011).
[59]T. Wang, K. C. Pitike, Y. Yuan, S. M. Nakhmanson, V. Gopalan, and B. Jalan, "Chemistry, growth kinetics, and epitaxial stabilization of Sn^{2+} in Sn-doped $SrTiO_3$ using $(CH_3)_6Sn_2$ tin precursor," APL Mater. **4**(12), 126111 (2016).

08 November 2026 01:46:08

© Author(s) 2026

[60]J. Gardner, A. Thakre, A. Kumar, and J. F. Scott, "Tin titanate—the hunt for a new ferroelectric perovskite," Rep. Prog. Phys. **82**(9), 092501 (2019).
[61]A. B. Mei, L. Miao, M. J. Wahila, G. Khalsa, Z. Wang, M. Barone, N. J. Schreiber, L. E. Noskin, H. Paik, T. E. Tiwald, Q. Zheng, R. T. Haasch, D. G. Sangiovanni, L. F. J. Piper, and D. G. Schlom, "Adsorption-controlled growth and properties of epitaxial SnO films," Phys. Rev. Mater. **3**, 105202 (2019).
[62]M. Barone, M. Foody, Y. Hu, J. Sun, B. Frye, S. S. Perera, B. Subedi, H. Paik, J. Hollin, M. Jeong, K. Lee, C. H. Winter, N. J. Podraza, K. Cho, A. Hock, and D. G. Schlom, "Growth of Ta_2SnO_6, A candidate wide-band-gap *p*-type oxide," J. Phys. Chem. C **126**, 3764–3775 (2022).
[63]M. Barone, C. Du, L. Radosavljevic, D. Werder, X. Pan, and D. G. Schlom, "Epitaxial synthesis of a vertically aligned two-dimensional van der Waals crystal: (110)-oriented SnO," Cryst. Growth Des. **22**, 7248–7254 (2022).
[64]C.-A. Chang, C. M. Serrano, L. L. Chang, and L. Esaki, "Effect of lattice mismatch on the electron mobilities of InAs grown on GaAs by MBE," J. Vac. Sci. Technol. **17**(2), 603–605 (1980).
[65]S. Ghosh, D. Leonhardt, and S. M. Han, "Effect of threading dislocation density and dielectric layer on temperature-dependent electrical characteristics of high-hole-mobility metal semiconductor field effect transistors fabricated from wafer-scale epitaxially grown p-type germanium on silicon substrates," J. Appl. Phys. **115**(9), 094507 (2014).
[66]J. L. Schroeder, A. S. Ingason, J. Rosén, and J. Birch, "Beware of poor-quality MgO substrates: A study of MgO substrate quality and its effect on thin film quality," J. Cryst. Growth **420**, 22–31 (2015).
[67]R. Uecker, B. Velickov, D. Klimm, R. Bertram, M. Bernhagen, M. Rabe, M. Albrecht, R. Fornari, and D. G. Schlom, "Properties of rare-earth scandate single crystals (Re = Nd−Dy)," J. Cryst. Growth **310**(10), 2649–2658 (2008).
[68]J. B. Nelson and D. P. Riley, "An experimental investigation of extrapolation methods in the derivation of accurate unit-cell dimensions of crystals," Proc. Phys. Soc. **57**(3), 160–177 (1945).
[69]S. Kikuchi, "Diffraction of cathode rays by Mica," Jpn. J. Phys. **5**(3061), 83–96 (1928).
[70]C. Guguschev, D. Klimm, M. Brützam, T. M. Gesing, M. Gogolin, H. Paik, A. Dittmar, V. J. Fratello, and D. G. Schlom, "Single crystal growth and characterization of Ba_2ScNbO_6—A novel substrate for $BaSnO_3$ films," J. Cryst. Growth **528**, 125263 (2019).
[71]N. A. Parker, S. Lee, K. Azizie, and D. G. Schlom, "High-mobility La-doped $BaSnO_3$ grown on Ba_2ScNbO_6" (unpublished).
[72]H. Yun, A. Prakash, T. Birol, B. Jalan, and K. A. Mkhoyan, "Dopant segregation inside and outside dislocation cores in Perovskite $BaSnO_3$ and reconstruction of the local atomic and electronic structures," Nano Lett. **21**, 4357–4364 (2021).

08 November 2026 01:46:08

© Author(s) 2026

Supplementary Material

High mobility La-doped $BaSnO_3$ thin films with sheet carrier concentrations relevant to transistors

Nicholas A. Parker,[1] Seungmin Lee,[1] Kathy Azizie,[1] Adedapo Oni,[2] George N. Kotsonis,[1] Jisung Park,[1] Hanjong Paik,[1,4,5] Jacary Sapp,[1] Jay R. Wright,[6] D. Jena,[1,7,8] H.G. Xing,[1,7,8] Dmitri A. Tenne,[6] Punyashloka Debashis,[3] Pratyush Buragohain,[3] Raseong Kim,[3] Rachel Steinhardt,[3] and Darrell G. Schlom[1,8,9]

[1] *Department of Materials Science and* [1]*Engineering, Cornell University, Ithaca, New York 14853, USA*

[2] *Quality and Reliability, Intel Corporation, Hillsboro, Oregon 97124, USA*

[3] *Intel Foundry Technology Research, Hillsboro, Oregon 97124, USA*

[4] *School of Electrical and Computer Engineering, University of Oklahoma, Norman, OK, 73019, USA*

[5] *Center for Quantum Research and Technology, University of Oklahoma, Norman, OK, 73019, USA*

[6] *Department of Physics, Boise State University, Boise, Idaho, 83725, USA*

[7] *School of Electrical and Computer Engineering, Cornell University, Ithaca, New York 14853, USA*

[8] *Kavli Institute at Cornell for Nanoscale Science, Ithaca, New York 14853, USA*

[9] *Leibniz-Institut für Kristallzüchtung, Max-Born-Str. 2, Berlin 12489, Germany*

[1] Author to whom correspondence should be addressed. Electronic mail: schlom@cornell.edu

Figure S1

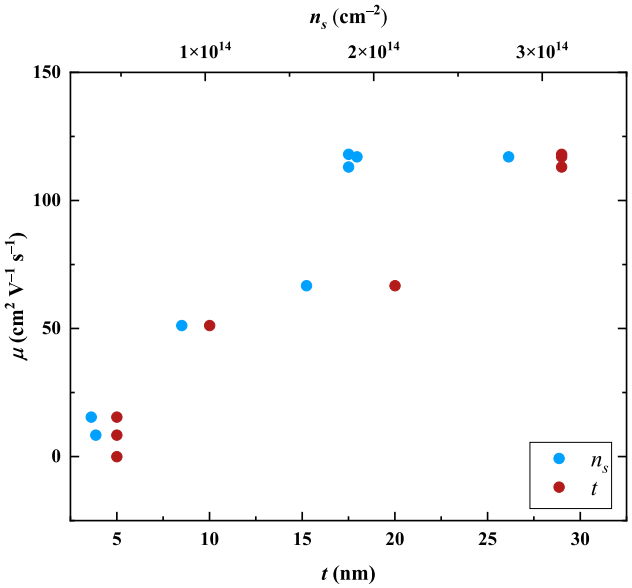


FIG. S1. A comparison of La-doped $BaSnO_3$ films grown on (100) MgO substrates with similar carrier concentrations ((8–9)×10^{19} cm^{-3}) and decreasing thickness, without UID $BaSnO_3$ buffer layers. The sample with $\mu = 0$ cm^2 V^{-1} s^{-1} and $n = 0$ cm^{-3} was insulating by two-point resistance.

Figure S1: A scatter plot showing the comparison of mobility to thickness as well as sheet carrier concentration. There are 8 La-doped $BaSnO_3$ films included ranging from 5 nm to 30 nm showing a decline in mobility with thickness.

Figure S2

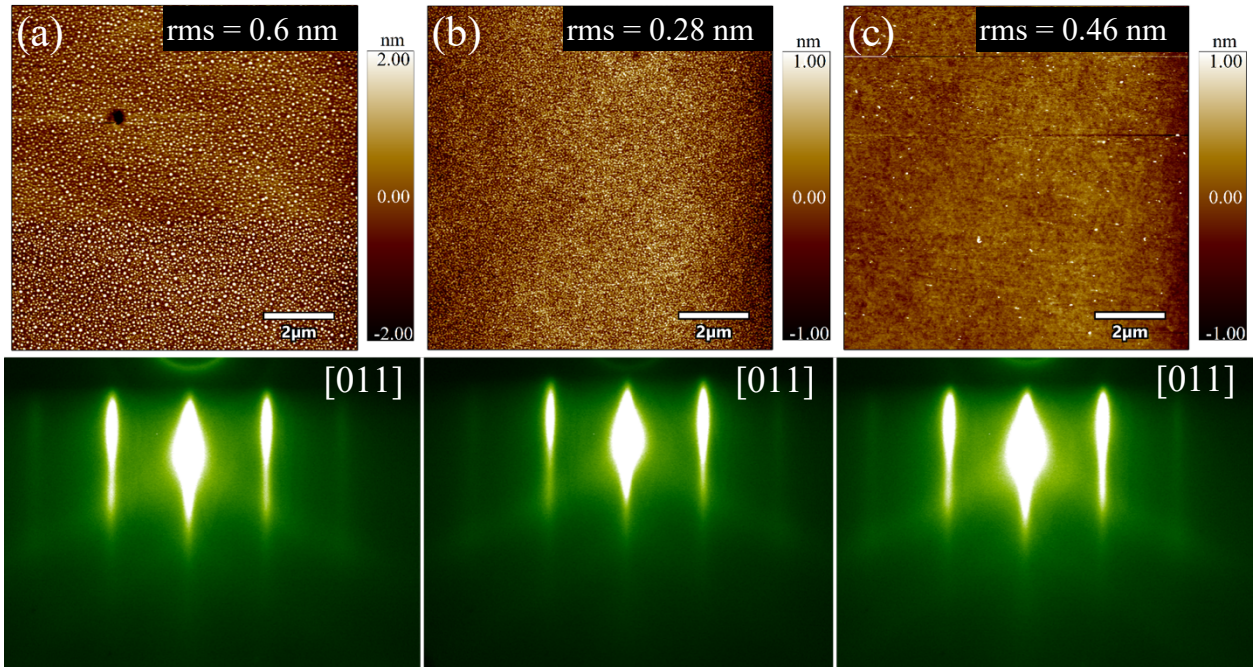


FIG. S2. AFM scans and corresponding RHEED images below them taken along the [011] azimuth from three 33 nm thick illustrative La-doped $BaSnO_3$ films grown at a SnO:Ba ratio of 4:1. (a) Ba-rich growth exhibiting the presence of small widely distributed precipitates on the surface of the film. (b) Stoichiometric growth. (c) Sn-rich growth illustrating the presence of larger, less distributed precipitates.

Figure S2: There are 3 panels containing AFM images with their corresponding RHEED images included below. The RHEED patterns are captured in kSA 400 using an RH15 electron gun from staib instruments and show an otherwise smooth surface by RHEED but some precipitates by AFM.

Figure S3

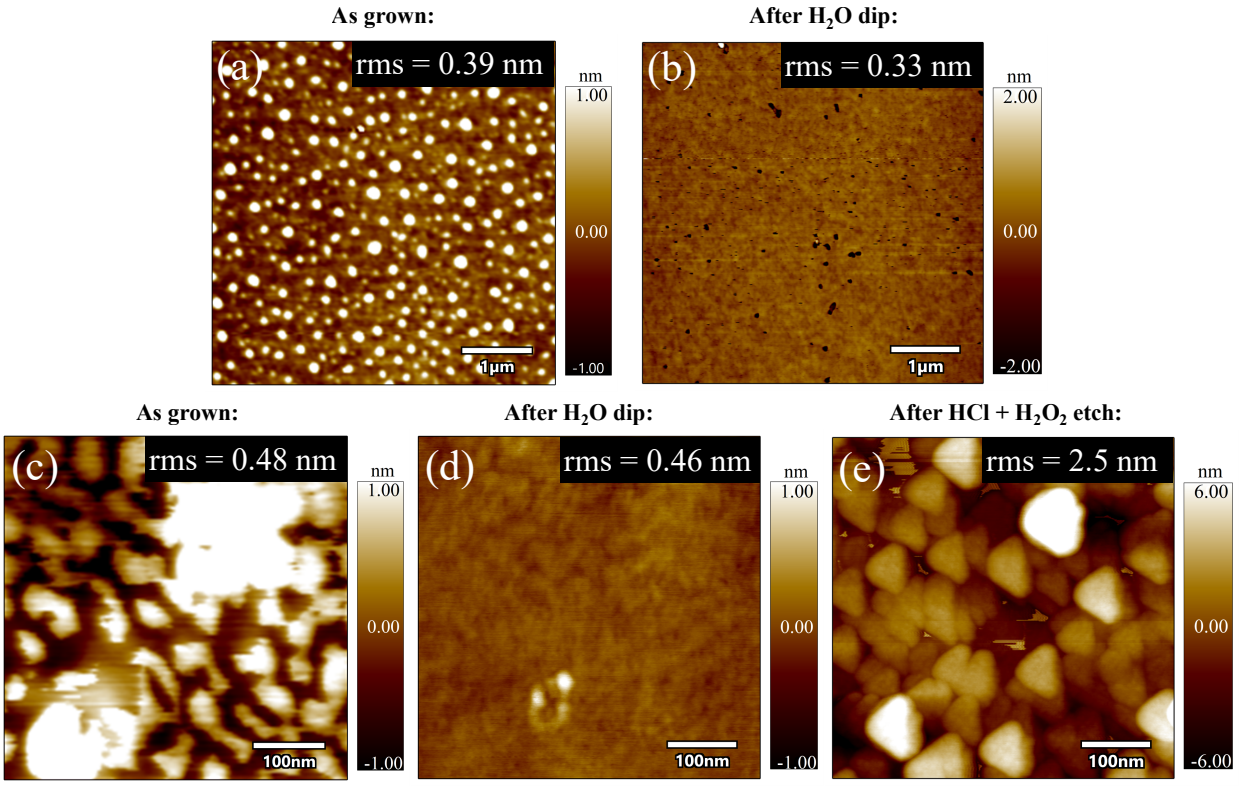


FIG. S3. AFM images of (a) initial surface of a Ba-rich film and (b) the resulting surface after dunking in DI water. (c) Initial surface of a Sn-rich sample, (d) the same sample after the same DI water dunk, and (e) the film after treatment with HCl + H_2O_2.

Figure S3: A comparison of 2 films, (1) with Ba-rich precipitates and (2) Sn-rich precipitates. The Sn-rich sample remained the same after dunking in water while the Ba-rich samples precipitates were removed. RMS values are in the upper right corner of each image.

Figure S4

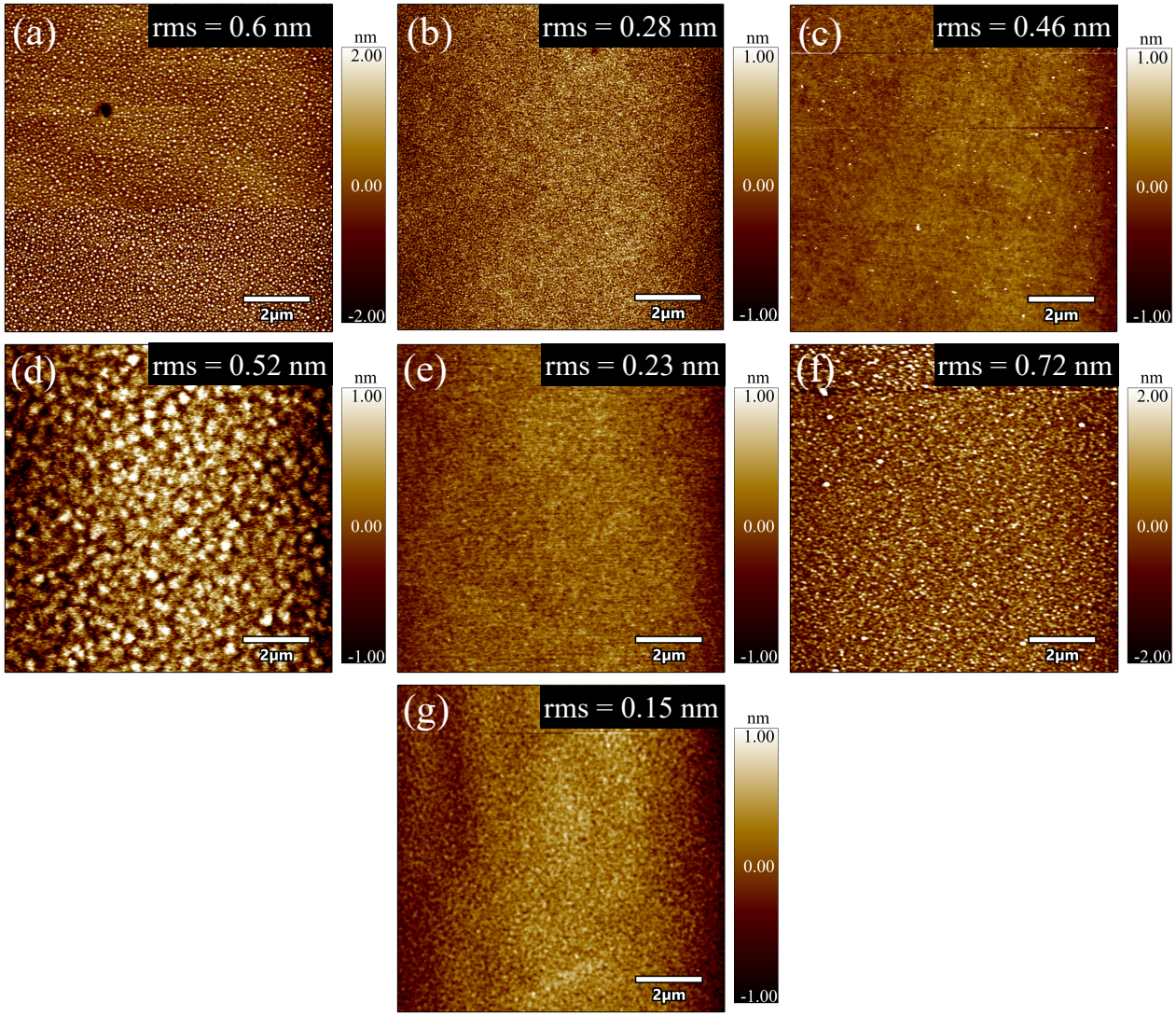


FIG. S4. A collection of AFM scans of samples grown with 4:1, 2:1, and 1.2:1 ratios of SnO:Ba comparing the roughness observed. Notably, the 1.2:1 ratio film has the lowest rms of 0.15 nm while the higher ratio samples of 2:1 and 4:1 have more spread in their roughness. From left to right in the 4:1 ratio row are the following mobilities and carrier concentrations: (a) 69 $cm^2\ V^{-1}\ s^{-1}$ with $n = 1.5\times10^{19}\ cm^{-3}$, (b) 95 $cm^2\ V^{-1}\ s^{-1}$ with $n = 1.7\times10^{19}\ cm^{-3}$, and (c) 75 $cm^2\ V^{-1}\ s^{-1}$ with $n = 1.7\times10^{19}\ cm^{-3}$. From left to right in the 2:1 ratio case: (d) 33.6 $cm^2\ V^{-1}\ s^{-1}$ with $n = 1.5\times10^{19}\ cm^{-3}$, (e) 74 $cm^2\ V^{-1}\ s^{-1}$ with $n = 1.9\times10^{19}\ cm^{-3}$, and (f) 67 $cm^2\ V^{-1}\ s^{-1}$ with $n = 8.9\times10^{18}\ cm^{-3}$.

Finally, the 1.2:1 ratio sample (g) had a mobility of 68 $cm^2\ V^{-1}\ s^{-1}$ and $n = 3\times10^{19}\ cm^{-3}$. All films are ~30–33 nm in thickness.

Figure S4: A comparison of 7 La-doped $BaSnO_3$ films with 3 from the 4:1 ratio, 3 from the 2:1 ratio, and 1 from the 1.2:1 ratio. The samples were grown on different days after the same calibration sequences.

Figure S5

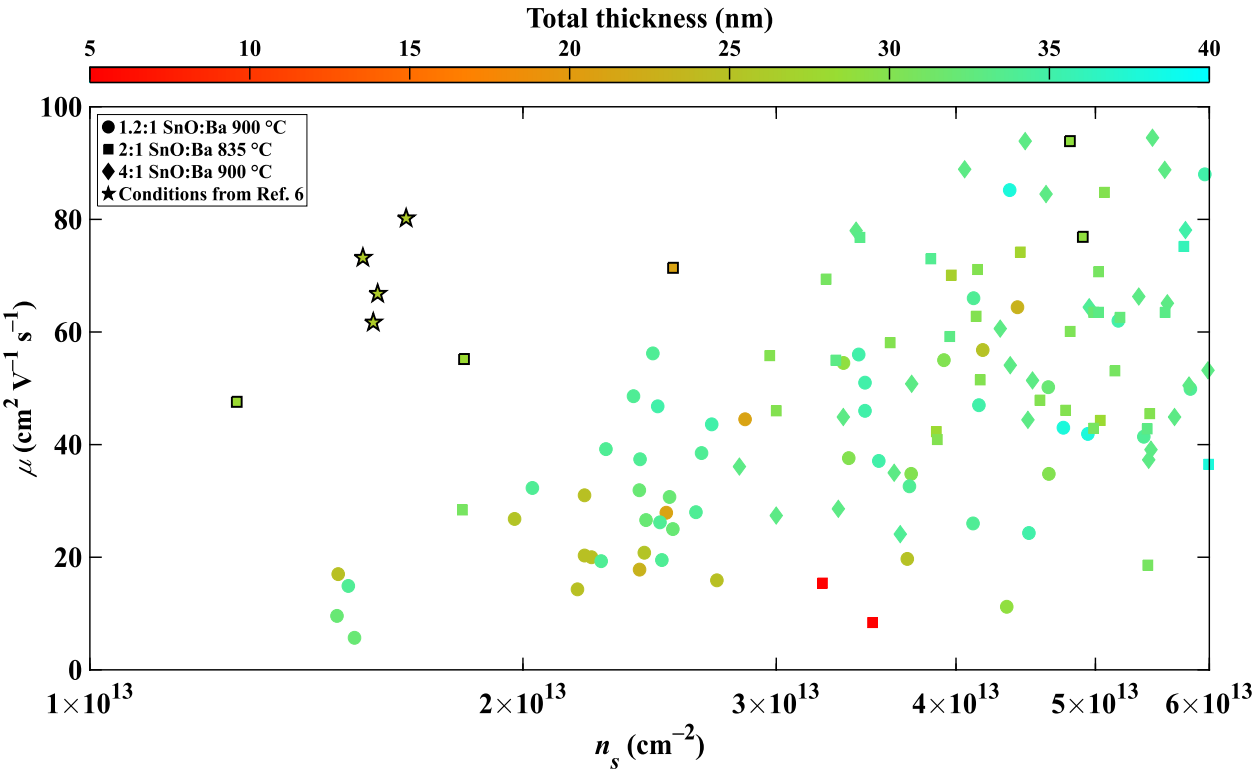


FIG. S5. A comparison of the same samples shown in Fig. 3(b) showing the comparison of μ vs. n_s for samples with total thickness under 40 nm. Stars are samples grown using the conditions from Ref. 6. The data points with black outlines have a UID $BaSnO_3$ buffer layer (~20 nm thick); those without a black outline have ≤1 U.C. UID $BaSnO_3$ buffer layer.

Figure S5: Close to 100 samples of La-doped $BaSnO_3$ grown using various conditions. A few thin samples with UID buffer layers retain higher mobilities at the same carrier concentrations.

Figure S6

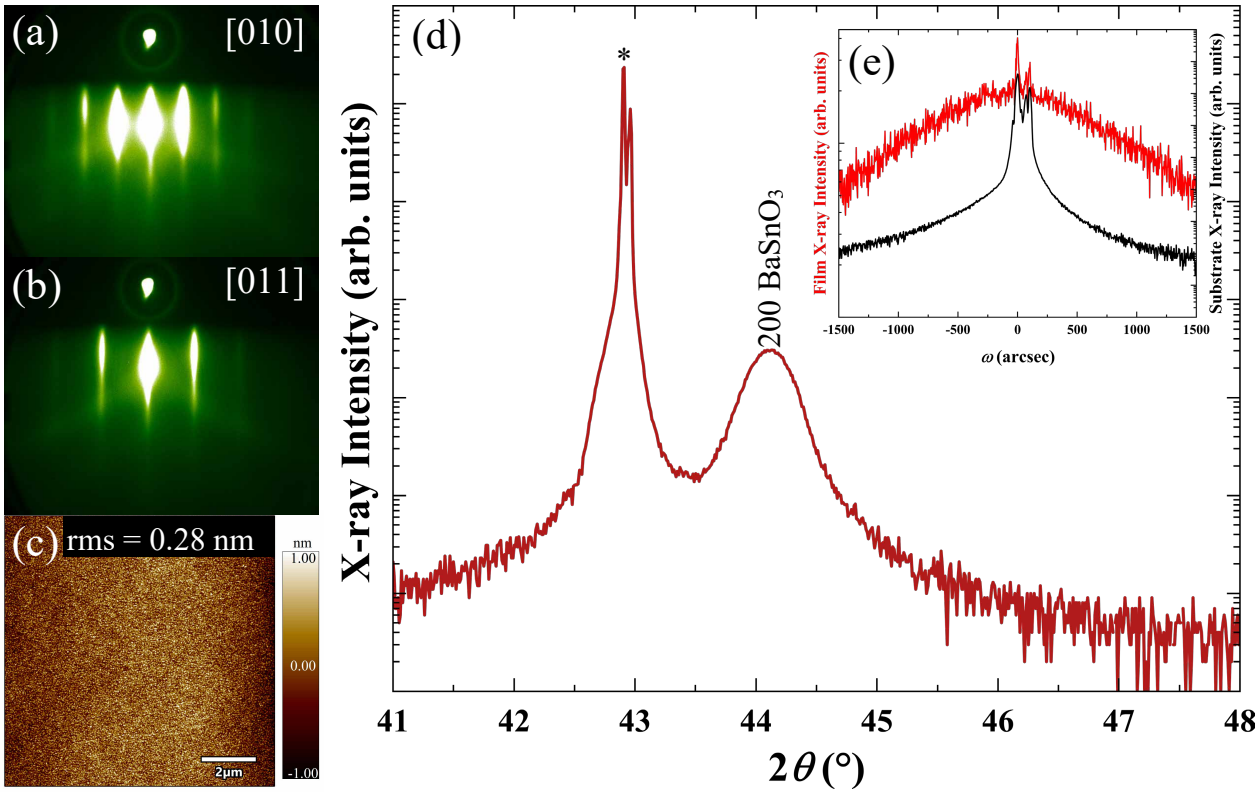


FIG. S6. Structural characterization of a 33 nm thick La-doped $BaSnO_3$ film with a room-temperature mobility of 95 $cm^2\ V^{-1}\ s^{-1}$ and a sheet carrier concentration of ~5.5×10^{13} cm^{-2} grown on a (100) MgO substrate without a UID $BaSnO_3$ buffer layer using the 4:1 SnO:Ba flux ratio. RHEED patterns at the end of growth taken along the (a) [010] and (b) [011] azimuths. (c) 10 × 10 μm^2 AFM scan exhibiting a rms roughness of 0.28 nm. (d) XRD θ-2θ scan and (e) overlapping rocking curve scans of the 200 La-doped $BaSnO_3$ peak and 200 MgO substrate peak.

Figure S6: Relevant characterization data processed for the 4:1 ratio of Ba:SnO. The data shows a lack of impurity by XRD, RHEED, and AFM.

Figure S7

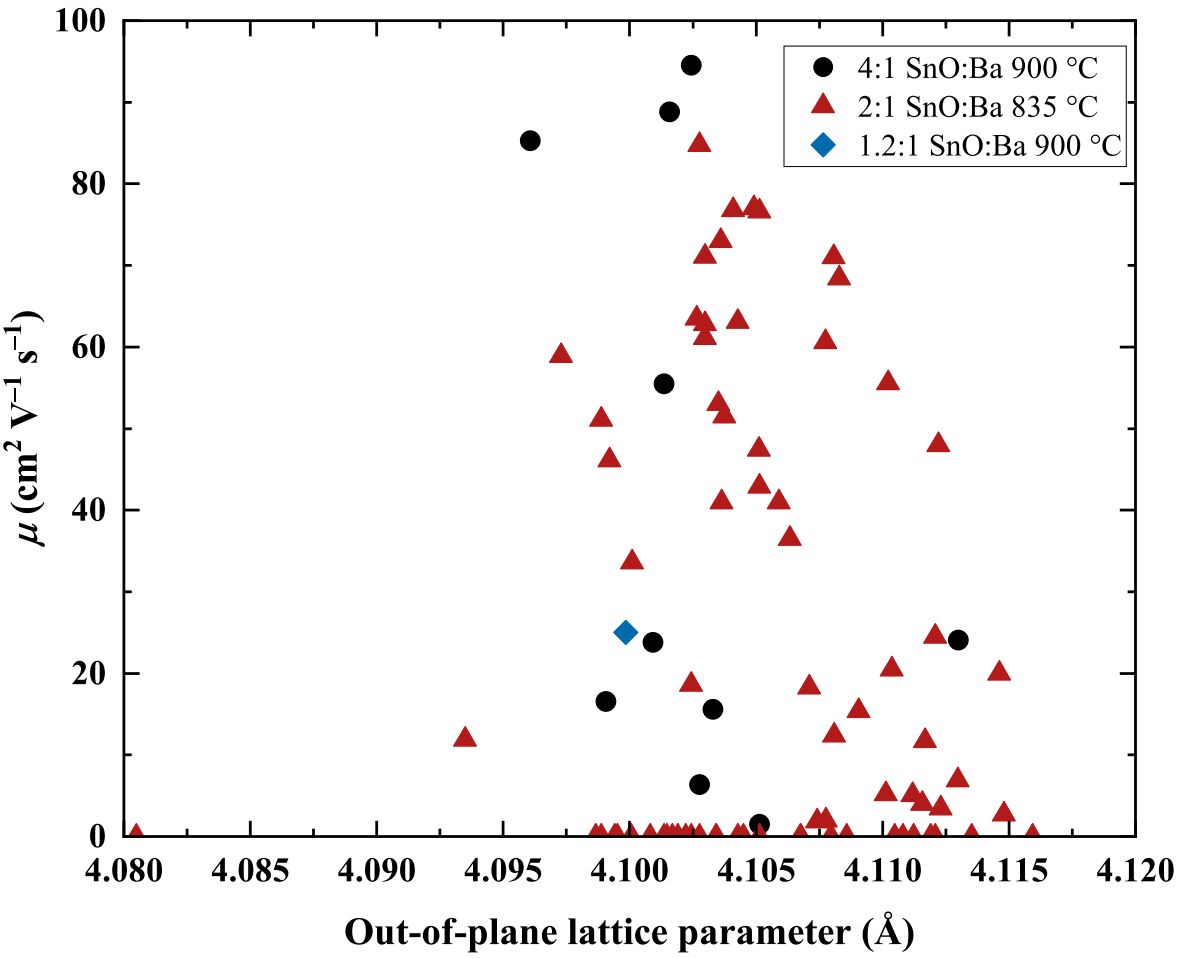


FIG. S7. A plot of mobility vs. out-of-plane lattice parameter for 97 samples from this study.

Figure S7: Mobilities for a few samples plotted against their lattice spacing measured from XRD. Most samples are from the 2:1 ratio which was the optimized condition for yield.

Figure S8

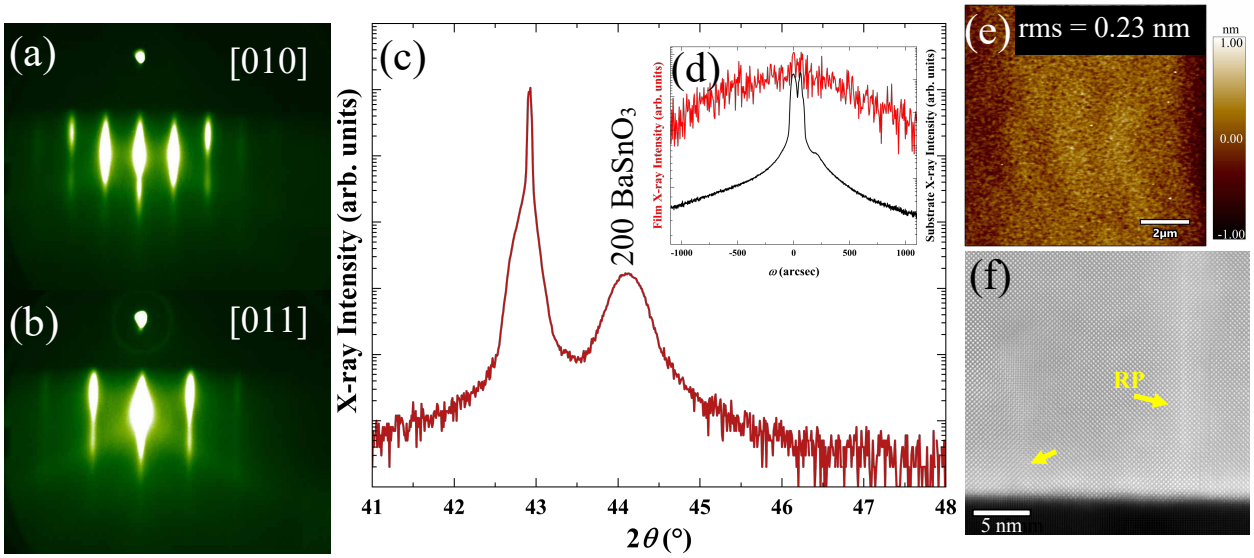


FIG. S8. Structural characterization of a 33 nm thick La-doped $BaSnO_3$ film with a room-temperature mobility of 77 $cm^2\ V^{-1}\ s^{-1}$ and a sheet carrier concentration of ~3.4×10^{13} cm^{-2} grown on a (100) MgO substrate without a UID $BaSnO_3$ buffer layer using the 2:1 SnO:Ba flux ratio. RHEED patterns taken after growth along the (a) [010] and (b) [011] azimuths. (c) XRD θ-2θ scan and (d) overlapping rocking curve scans of the 200 La-doped $BaSnO_3$ peak and 200 MgO substrate peak. (e) 10×10 μm^2 AFM scan exhibiting a rms roughness <0.25 nm. A cross-sectional HAADF-STEM image is displayed in (f) showing a threading dislocation and RP fault as indicated by the yellow arrows.

Figure S8: Relevant characterization data processed for the 2:1 ratio of Ba:SnO. The data shows a lack of impurity by XRD, RHEED, and AFM. TEM shows the presence of RP defects illustrated by arrows.

Figure S9

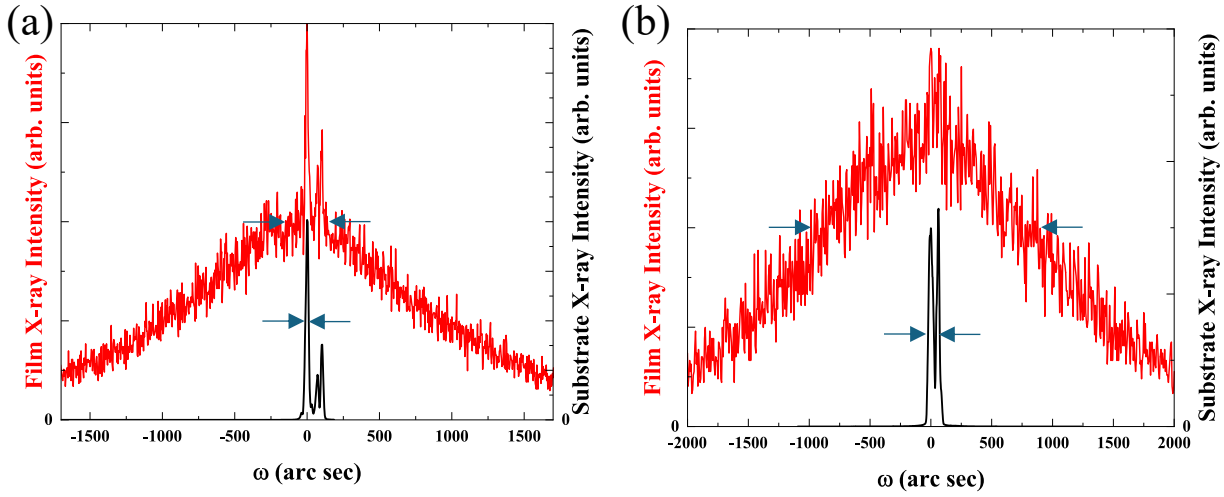


FIG. S9. A linear scale representation of the same ω rocking curves shown in (a) Fig. S6 and (b) Fig.S8. The arrows indicate the FWHM.

Figure S9: Rocking curve plots from previous figures with a linear scale. Arrows are blue and show both the film and substrate FWHM.

Figure S10

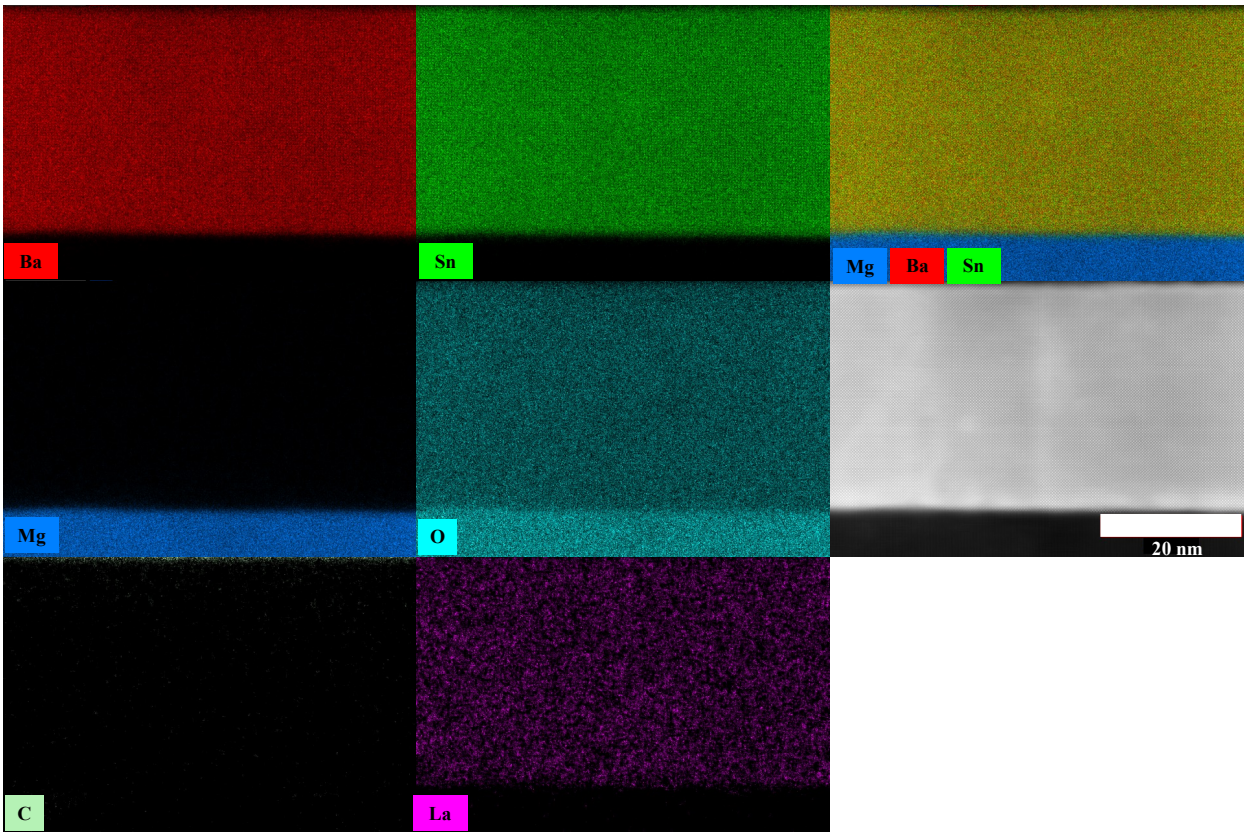


FIG. S10. EDX compositional analysis for various elements including barium, carbon, tin, lanthanum, magnesium, and oxygen. A high resolution HAADF-STEM image accompanies the EDX scan in the right center.

Figure S10: 7 EDX compositional plots included with the corresponding area scanned by STEM.

Figure S11

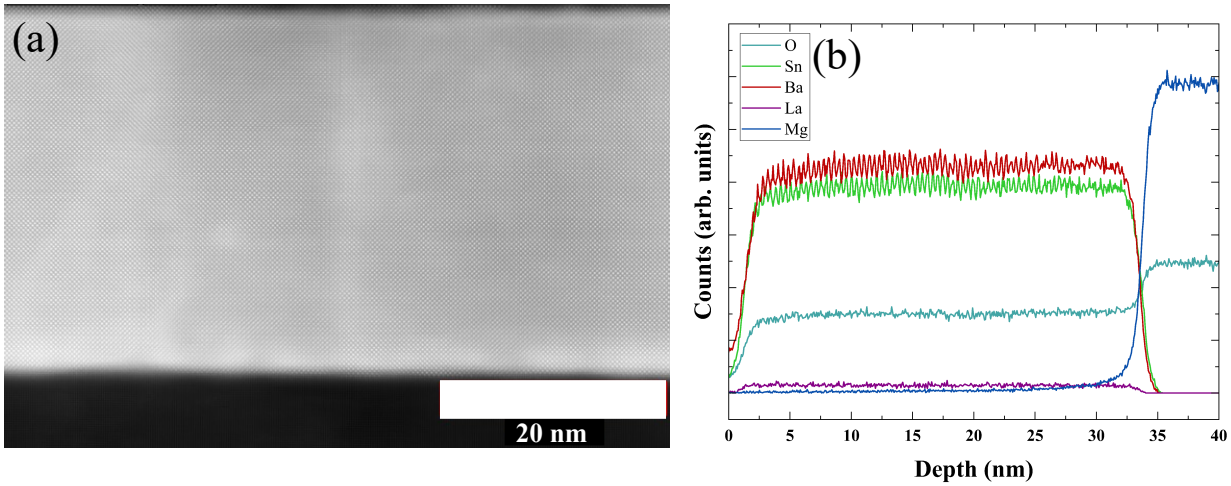


FIG. S11. (a) A low-magnification cross-sectional HAADF-STEM image of the La-doped $BaSnO_3$ film shown in Fig. S8 with (b) an EDX scan of the film.

Figure S11: A STEM images adjacent to an EDX scan for the same area showing the uniformity of the La-doped $BaSnO_3$ film.

Figure S12

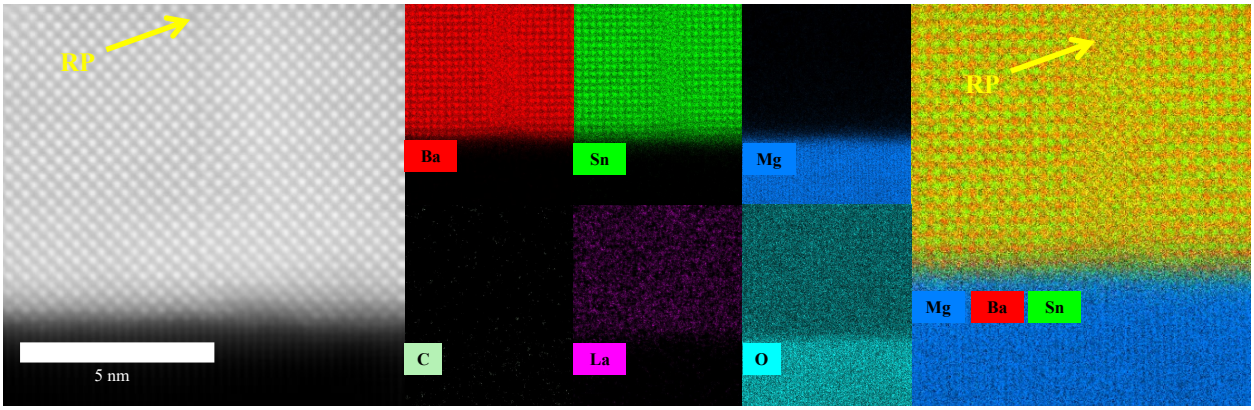


FIG. S12. EDX compositional analysis locally surrounding an RP fault (arrowed) for various elements including barium, carbon, tin, lanthanum, magnesium, and oxygen. A high-resolution cross-sectional HAADF-STEM image accompanies the EDX scan in the bottom right image.

Figure S12: STEM images included with EDX compositional analysis for a La-doped $BaSnO_3$ film and focus on the RP defect present.

Figure S13

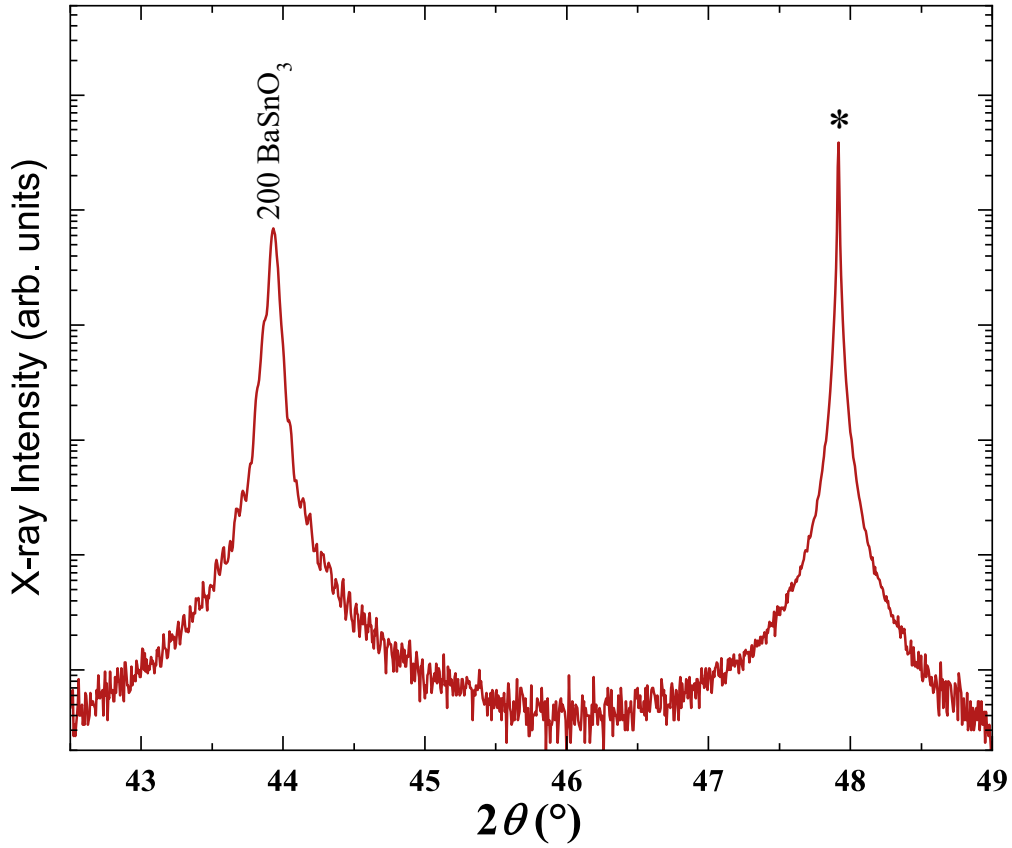


FIG. S13. θ-2θ XRD scan of the 70 nm thick La-doped $BaSnO_3$ film found to exhibit a room-temperature Hall mobility of 194 $cm^2\ V^{-1}\ s^{-1}$. This film was grown using the conditions found in Ref. 6 on a 140 nm thick UID $BaSnO_3$ buffer layer on a (100) $LaAlO_3$ substrate (*).

Figure S13: Rebinned XRD data for a thick La-doped $BaSnO_3$ sample including a thick UID buffer layer.

Figure S14

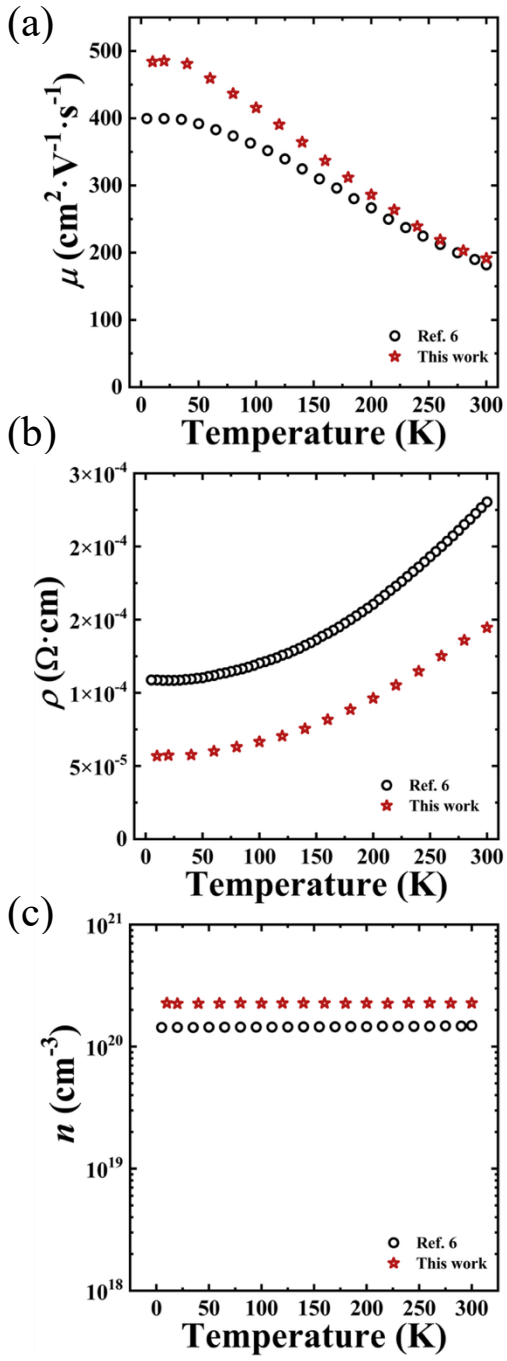


FIG. S14. Temperature-dependent (a) Hall mobility, (b) resistivity, and (c) carrier concentration measurements of the same 70 nm thick La-doped $BaSnO_3$ film characterized in Fig. S13.

Figure S14: Corresponding temperature dependent hall data to the XRD data of the sample included in Figure S14.

Figure S15

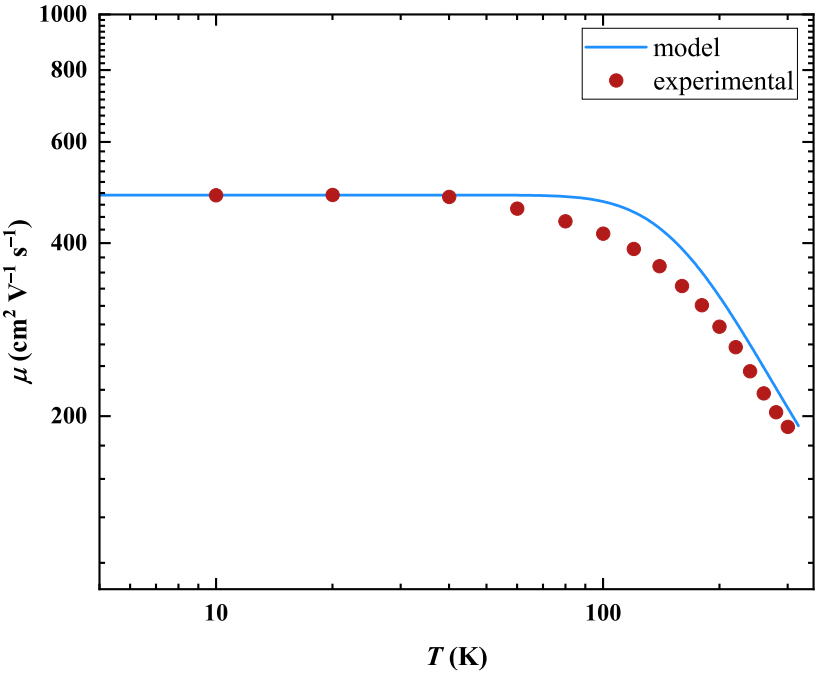


FIG. S15. Comparison of experimentally measured electron mobility of the same 70 nm thick La-doped $BaSnO_3$ film characterized in Figs. S13 and S14. The measured mobility of the La-doped $BaSnO_3$ film is shown as red circles together with a theoretical model shown as a light blue solid line.

Figure S15: A model comparison to experimental data for the same sample discussion in Figure S13 and Figure S14. The model follows closely with some deviation around 100 K.

We have compared the measured temperature-dependent mobility in the $BaSnO_3$ sample with the highest mobility in this study with a theoretical model that accounts for optical phonon scattering and impurity scattering. Figure S15 shows this comparison. We have used a single optical phonon energy of 51 meV for our calculation. For $BaSnO_3$, scattering from three longitudinal optical (LO) phonon branches are active, at 18 meV, 51 meV, and 88 meV, as discussed in Krishnaswamy et al.[1] Of these three LO phonon modes, scattering from the 51 meV LO mode dominates the scattering rate at $T > 100$ K, and the 18 meV LO mode dominates for $T < 100$ K. Because the low temperature electron mobility is limited to ~ 484 $cm^2\ V^{-1}\ s^{-1}$, the 18 meV phonon mode scattering limited mobility, which dominates < 100 K for mobilities > 10,000 $cm^2\ V^{-1}\ s^{-1}$ is not observable. Thus, the use of a single phonon mode is justified. The discrepancy between the theory and the experiment around 100 K is due to another temperature-dependent scattering mechanism that we have not yet identified. The measured mobile electron density at $n \sim 2.27 \times 10^{20}$ cm^{-3} is degenerate and nearly constant with temperature. As shown in this work, Ruddlesden-Popper type defect scattering could be active in the samples studied here. Typically inactive TO phonon mode scattering of electrons could play a role as they have been seen to do in other perovskite oxides such as $SrTiO_3$,[2] though the electron bandstructure of $BaSnO_3$ near the conduction band minimum follows a different symmetry than $SrTiO_3$. A study of mobility limitations from scattering by Ruddlesden-Popper defects, potentially TO modes if they are active in $BaSnO_3$ is a topic for future study.

References

[1] K. Krushnaswamy, B. Himmetoglu, Y. Kang, A. Janotti, and C. G. Van de Walle, "First-principles analysis of electron transport in $BaSnO_3$," Phys. Rev. B **95**, 205202 (2017).

[2] A. Verma, A. P. Kajdos, T. A. Cain, S. Stemmer, and D. Jena, "Intrinsic Mobility Limiting Mechanisms in Lanthanum-Doped Strontium Titanate," Phys. Rev. Lett. **112**, 216601 (2014).